CONTINUOUS FLOW SELECTIVE HYDROGENATION OF 5-HYDROXYMETHYLFURFURAL

TO 2.5-DIMETHYLFURAN USING Pd-Cu/REDUCED GRAPHENE OXDE CATALYSTS

Miss Sareena Mhadmhan

จุฬาลงกรณ์มหาวิทยาลัย
CHULALONGKORN UNIVERSITY

A Dissertation Submitted in Partial Fulfillment of the Requirements

for the Degree of Doctor of Philosophy in Petrochemistry and Polymer Science

Field of Study of Petrochemistry and Polymer Science

Faculty of Science

Chulalongkorn University

Academic Year 2019

Copyright of Chulalongkorn University

ไฮโดรจิเนชันแบบเลือกจำเพาะด้วยการไหลแบบต่อเนื่องของ 5-ไฮดรอกซีเมทิลเฟอร์ฟูรัลเป็น
2,5-ไดเมทิลฟูแรนโดยใช้ตัวเร่งปฏิกิริยาแพลเลเดียม-คอปเปอร์/รีดิวซ์กราฟีนออกไซด์

น.ส.สารีน่า หมัดหมาน

Thesis Title	CONTINUOUS FLOW SELECTIVE HYDROGENATION OF 5-HYDROXYMETHYLFURFURAL TO 2.5-DIMETHYLFURAN USING Pd-Cu/REDUCED GRAPHENE OXDE CATALYSTS
By	Miss Sareena Mhadmhan
Field of Study	Petrochemistry and Polymer Science
Thesis Advisor	Associate Professor PRASERT REUBROYCHAROEN, Ph.D.

Accepted by the Faculty of Science, Chulalongkorn University in Partial Fulfillment of the Requirement for the Doctor of Philosophy

.... Dean of the Faculty of Science

(Professor POLKIT SANGVANICH, Ph.D.)

DISSERTATION COMMITTEE

.... Chairman

(Associate Professor NAPIDA HINCHIRANAN, Ph.D.)

.... Thesis Advisor

(Associate Professor PRASERT REUBROYCHAROEN, Ph.D.)

.... Examiner

(Associate Professor Chawalit Ngamcharussrivichai, Ph.D.)

.... Examiner

(Assistant Professor WARINTHORN CHAVASIRI, Ph.D.)

.... Examiner

(Duangamol Tungasmita, Ph.D.)

.... External Examiner

(Assistant Professor Chanatip Samart, Ph.D.)

สารีน่า หมัดหมาน : ไฮโดรจิเนชันแบบเลือกจำเพาะด้วยการไหลแบบต่อเนื่องของ 5-ไฮดรอกซีเมทิลเฟอร์ฟูรัลเป็น 2,5-ไดเมทิลฟูแรนโดยใช้ตัวเร่งปฏิกิริยาแพลเลเดียม-คอปเปอร์/รีดิวซ์กราฟีนออกไซด์. (CONTINUOUS FLOW SELECTIVE HYDROGENATION OF 5-HYDROXYMETHYLFURFURAL TO 2.5-DIMETHYLFURAN USING Pd-Cu/REDUCED GRAPHENE OXDE CATALYSTS) อ.ที่ปรึกษาหลัก : รศ. ดร.ประเสริฐ เรียบร้อยเจริญ

2,5-ไดเมทิลฟูแรน ถูกพิจารณาเป็นเชื้อเพลิงชีวภาพที่ผลิตได้จากชีวมวล หลายงานวิจัยที่ผ่านมาศึกษาการผลิต 2,5-ไดเมทิลฟูแรน จากไฮโดรจิเนชันของ 5-ไฮดรอกซีเมทิลเฟอร์ฟูรัล อย่างไรก็ตามงานวิจัยส่วนใหญ่ยังคงศึกษาภายใต้ภาวะการใช้ไฮโดรเจนความดันสูง ใช้ระยะเวลาในการทำปฏิกิริยานาน และปฏิกิริยายังคงศึกษาในเครื่องปฏิกรณ์แบบแบตช์ งานวิจัยนี้ใช้ตัวเร่งปฏิกิริยาโลหะผสมแพลเลเดียม-คอปเปอร์ บนตัวรองรับรีดิวซ์กราฟีนออกไซด์ถูกใช้สำหรับการไฮโดรจิเนชันแบบเลือกจำเพาะของ 5-ไฮดรอกซีเมทิลเฟอร์ฟูรัลเป็น 2,5-ไดเมทิลฟูแรน โดยใช้ 2-โพรพานอลเป็นแหล่งไฮโดรเจน ภายใต้ระบบการไหลแบบต่อเนื่อง ตัวเร่งปฏิกิริยาที่สังเคราะห์ทั้งหมดถูกนำมาทดสอบลักษณะเฉพาะด้วยเทคนิคต่างๆ ดังนี้ การดูดซับทางกายภาพด้วยไนโตรเจน, กล้องจุลทรรศน์อิเล็กตรอนแบบส่องกราด-เอนเนอร์จีดิสเพอร์ซีฟเอกซ์เรย์สเปกโทรสโกปี (SEM-EDX), เอกซ์เรย์ดิฟแฟรกชัน (XRD), เอกซเรย์โฟโตอิเล็กตรอนสเปกโทรสโกปี (XPS), กล้องจุลทรรศน์อิเล็กตรอนแบบส่องผ่าน(TEM) และโปรแกรมอุณหภูมิรีดักชันด้วยไฮโดรเจน (H_2-TPR) ภายใต้ภาวะการทำปฏิกิริยาที่เหมาะสม ตัวเร่งปฏิกิริยา 1Pd-10Cu/RGO ให้ค่าร้อยละการเปลี่ยน 5-ไฮดรอกซีเมทิลเฟอร์ฟูรัลเท่ากับ 96 ค่าร้อยละการเกิด 2,5-ไดเมทิลฟูแรนเท่ากับ 95 และเสถียรภาพของตัวเร่งปฏิกิริยาที่ดี จากผลการวิเคราะห์ลักษณะเฉพาะของตัวเร่งปฏิกิริยาด้วยเทคนิค XRD และ XPS พบอัลลอยของแพลเลเดียม-คอปเปอร์ ซึ่งเป็นส่วนที่ช่วยเพิ่มกัมมันตภาพและเสถียรภาพของตัวเร่งปฏิกิริยาในการเปลี่ยน 5-ไฮดรอกซีเมทิลเฟอร์ฟูรัลเป็น 2,5-ไดเมทิลฟูแรน นอกจากนี้งานวิจัยได้ศึกษาผลของอุณหภูมิ ความดัน และอัตราการไหลของสารตั้งต้นต่อประสิทธิภาพของตัวเร่งปฏิกิริยา และจากผลการศึกษาเสถียรภาพของตัวเร่งปฏิกิริยาเป็นเวลา 8 ชั่วโมง พบว่าตัวเร่งปฏิกิริยาให้ค่าร้อยละการเปลี่ยน 5-ไฮดรอกซีเมทิลเฟอร์ฟูรัลเท่ากับ 67 และค่าร้อยละการเกิด 2,5-ไดเมทิลฟูแรนเท่ากับ 65

สาขาวิชา	ปิโตรเคมีและวิทยาศาสตร์พอลิเมอร์	ลายมือชื่อนิสิต ....
ปีการศึกษา	2562	ลายมือชื่อ อ.ที่ปรึกษาหลัก ....

5972892523 : MAJOR PETROCHEMISTRY AND POLYMER SCIENCE

KEYWORD: 5-Hydroxymethylfurfural, Biofuel, Continuous flow, Pd-Cu Catalyst

Sareena Mhadmhan : CONTINUOUS FLOW SELECTIVE HYDROGENATION OF 5-HYDROXYMETHYLFURFURAL TO 2.5-DIMETHYLFURAN USING Pd-Cu/REDUCED GRAPHENE OXDE CATALYSTS. Advisor: Assoc. Prof. PRASERT REUBROYCHAROEN, Ph.D.

2,5-Dimethylfuran (DMF) has been considered a promising biofuel, potentially derived from biomass. There have been various reports on DMF production from hydrogenation of 5-hydroxymethylfurfural (HMF). However, most reports employed high hydrogen pressure, long reaction times, and reactions under batch reactor. In this study, Pd-Cu bimetallic catalysts incorporated on reduced graphene oxide (RGO) were used for hydrogenation of HMF to DMF using 2-propanol as hydrogen donor under continuous flow system. Synthesized catalysts were characterized by N_2 physisorption, scanning electron microscopy-energy dispersive X-ray spectroscopy (SEM-EDX), X-ray diffraction (XRD), X-ray photoelectron spectroscopy (XPS), transmission electron microscopy (TEM), and temperature programmed reduction of hydrogen (H_2-TPR) techniques. 10Cu1Pd/RGO exhibited 96% HMF conversion with 95% DMF yield under optimum reaction conditions with good stability with time on stream. XRD and XPS results pointed to the presence of a palladium–copper alloy, which could enhance both the activity and especially the stability in the conversion of HMF toward DMF. The effect of temperature, pressure, and feed flow rate were also investigated on the catalytic performance. The stability of catalyst was tested for 8 h time on stream, where it was found that the catalyst provided 67% HMF conversion with 65% DMF yield.

Field of Study:	Petrochemistry and Polymer Science	Student's Signature ....
Academic Year:	2019	Advisor's Signature ....

ACKNOWLEDGEMENTS

TABLE OF CONTENTS

LIST OF TABLES

LIST OF FIGURES

จุฬาลงกรณ์มหาวิทยาลัย

CHULALONGKORN UNIVERSITY

LIST OF ABBRIVIATION

HMF	5-Hydroxymethylfurfural
MF	5-Methylfurfural
MFA	5-Methylfurfuryl alcohol
FA	Furfuryl alcohol
DHMF	2,5-Dihydroxymethyl furan
DMF	2,5-Dimethylfuran
DFF	2,5-Diformylfuran
DMTHF	2,5-Dimethyltetrahydrofuran
DHMTHF	2,5-Di(hydroxymethyl)tetrahydrofuran
Cu	Copper
Pd	Palladium
RGO	Reduced graphene oxide
N_2	Nitrogen
H_2	Hydrogen
Ar	Argon
T	Temperature
P	Pressure
°C	Degree Celsius
XRD	X-ray Diffraction
XPS	X-ray photoelectron spectroscopy
TPR	Temperature-programmed reduction
SEM	Scanning electron microscopy
EDX	Energy dispersive X-ray spectroscopy
TEM	Transmission electron microscopy
GC	Gas chromatograph
TCD	Thermal conductivity detector

FID	Flame ionization detector
MS	Mass spectrometry
Atm	Atmospheric pressure
µm	Micron meter
cm^3	Cubic centimeter
mL	Milliliter
min	Minute (s)
g	Gram
wt.%	Weight percent
wt.	Weight
et al.	And others
Mw.	Molecular weight

CHAPTER I

INTRODUCTION

1.1 Statement of problem

Biomass, as sustainable resource, can be transformed into high value-added chemicals and alternative fuels. As potential biofuel compound, 2,5-dimethylfuran (DMF) has promising physical and chemical properties due to high energy density (30 $kJ \cdot cm^{-3}$) and high octane number (RON=119). DMF can be used as blend fuel, produced via selective hydrogenation of 5-hydroxymethylfurfural (HMF) obtained from lignocellulose dehydration. During HMF hydrogenation, several side reactions have been reported to take place including ring opening, ring hydrogenation, total hydrogenation and partial hydrogenation. Thus, catalyst development for the highly selective hydrogenation of HMF toward DMF still remains a significant challenge. Various noble metals such as Pd, Ru, Pt, and Rh have been reported in the hydrogenation of HMF toward DMF. Ru and Pd provided the best reported performance. However, Pd-based catalysts provided moderate DMF selectivity because Pd is highly active for the hydrogenation of C=O groups and C=C bonds of furan ring as well as hydrogenolysis of C-O bonds. Moreover, the high costs of Pd had limited their scale-up application. The development of low-cost catalysts with high selectivity to DMF in this reaction is still in progress. To minimize costs, the combination between palladium metal and a second (transition) metal is highly desirable as it can reduce palladium loading and maximize activity/selectivity to DMF. Pd-Cu catalysts have been extensively employed in reactions including CO_2 hydrogenation and hydrogenation of furfural to furfuryl alcohol. In general, Cu-based catalysts exhibited high selectivity for the

hydrogenation of carbonyl group, leaving unreduced C=C bonds from the furan ring due to strong repulsion between the surface of Cu (111) and the furan ring. The addition of Cu into Pd-based catalyst could probably enhance DMF selectivity. Additionally, the use of alcohols as hydrogen donors has been extensively reported due to their availability and the possibility to safely and effectively conduct transfer hydrogenation reactions, with 2-propanol being most often selected alcohol for such chemistries. In addition, the hydrogenation of HMF to DMF of previous literature works was only studied under batch conditions. Continuous flow has many advantages as compared to batch systems including faster and easy scale-up and a more controllable setup to maximize and fine-tune activity ad selectivity to target products.

In this work, monometallic Pd and Cu and Pd-Cu bimetallic catalysts were prepared on reduced graphene oxide (RGO), fully characterized and subsequently investigated in the selective hydrogenation of HMF to DMF using 2-propanol as hydrogen donor under continuous flow conditions. The influence of reaction temperature, pressure, and feed flow rate were evaluated to maximize DMF yields.

1.2 Scope of research

The research procedures were carried out as follows:

1. Review literature

2. Prepare Pd, Cu and Pd-Cu supported on reduced graphene oxide (RGO) catalysts by co-impregnation method

3. Study the effect of different catalysts on the selective hydrogenation of HMF toward DMF under continuous-flow reactor and analyze the liquid product by gas chromatography-thermal conductivity detector and flame ionization detector (GC-TCD&FID) and gas chromatography-mass spectrometry (GC-MS)

4. Study the effects of reaction condition on conversion of 5-hydroxymethylfurfural (HMF) and product distribution in hydrogenation of HMF. The investigated parameters are:

- Temperature (140, 160, 180, and 200 ℃)

- Feed flow rate (0.2, 0.3 and 0.5 mL·min^{-1})

- Pressure (0, 15 and 30 bar)

5. Study catalytic stability under optimum conditions

6. Characterize fresh and spent catalysts using techniques as follows:

- Nitrogen adsorption measurement

- Powder X-ray diffraction (XRD)

- Temperature-programmed reduction of H$_2$ (H$_2$-TPR)

- Scanning electron microscopy (SEM)

- Transmission electron microscopy (TEM)

- Energy dispersive X-ray spectroscopy (EDX)

- X-ray photoelectron spectroscopy (XPS)

7. Summarize the results

8. Write manuscripts and dissertation

1.3 Objective

To study effect of reduced graphene oxide-supported monometallic and bimetallic catalysts on selective hydrogenation of 5-hydroxymethylfurfural toward 2,5-dimethylfuran under continuous flow regime.

CHAPTER II

THEORY AND LITERATURE REVIEW

2.1 Energy demand

Fossil fuel sources are natural gas, petroleum, coal, oil and bitumen which were formed in early geological periods. They are not renewable energy sources and are distributed in specific geographical locations. Fossil fuel is the primary energy source used, which is mostly consumed in an industry and transportation sectors as displays in Figure 1 [1]. However, the abundant fossil resources are reducing steadily in addition to instability in price, attention has been shifted to alternative energy sources to supplement the increasing demand. The world will require 52% more energy in 2040 than in 2018 (Figure 1). As can be seen in Figure 1, the current dominant energy sources are oil, coal and natural gases. However, compared with nuclear and renewables, which have both increased by 3-4%, fossil fuel resources will be further depleted by 2040 [2]. It is estimated that the use of petroleum is 10^5 faster than the speed with which it can be replaced by nature. As a result, the development of renewable energy resources becomes a major requirement so as to supply the future global energy demand.
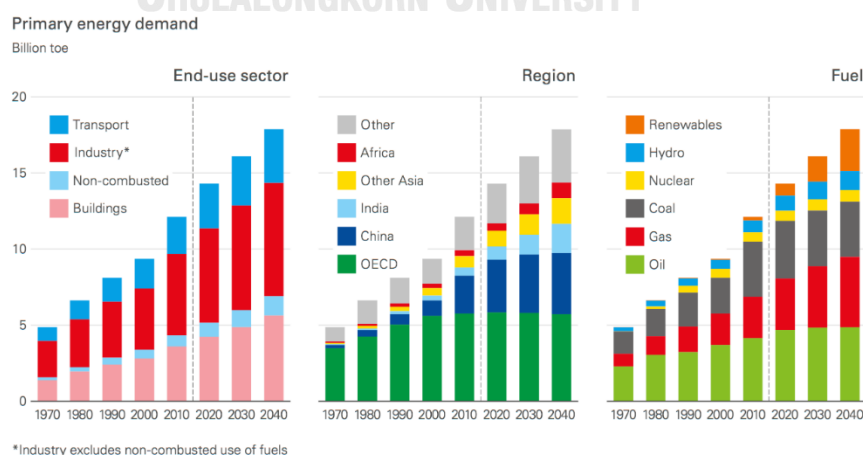
Figure 1 Primary energy demand [2].

Moreover, the concerning of global warming and environmental pollution, renewable and alternative energy sources need to reduce greenhouse gas emissions from the consumption of fossil fuels. Currently, fossil fuel is vital as materials for energy supply, however; it is non-renewable source that results in climate change. Generally, the combustion of fossil fuel causes the carbon dioxide emission, resulting in global warming [3]. Figure 2 exhibits the global emission of carbon dioxide that is extremely increasing. The emission of carbon dioxide from coal presents the highest as compared to liquids and natural gas. Owing to the increasing of energy demand, the concerning of global warming and unstable prices of oil, the use of biomass as energy supply is growing significantly. Thus, biofuel is considered as a good option for fuel consumption because it is renewable, biodegradable and generate lower greenhouse gases amounts
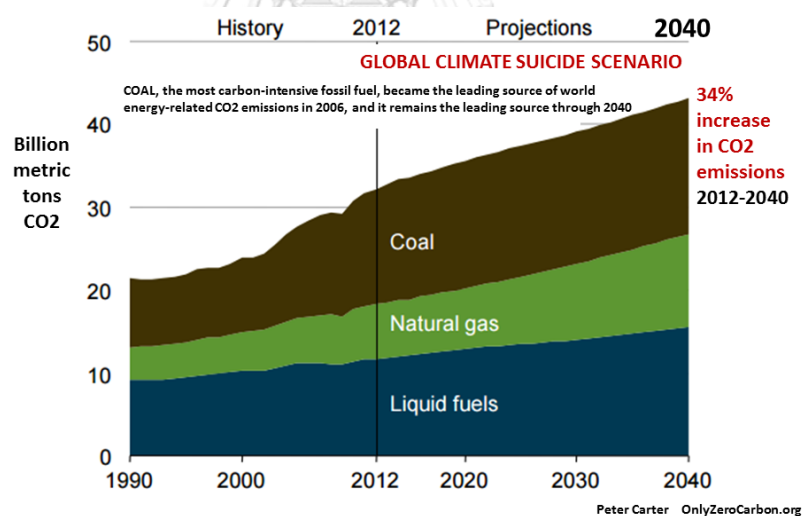
Figure 2 Global emission of carbon dioxide by fuel type [4].

2.2 2,5-Dimethylfuran as a new generation biofuel

The careless use and rapid depletion of fossil fuels makes renewable energy sources the only currently viable option for the near future. The vast infrastructure based on the use of liquid fossil fuels for transportation favours their direct

replacement with biofuels produced from biomass feedstock [5, 6]. Many different techniques exist to convert biomass into biofuels or its precursors, including, gasification, hydrolysis, transesterification, and pyrolysis [6]. Additionally, the production of biofuels together with bioproducts can provide new employment and income opportunities in rural areas. A shift to alternative biofuels and green processes to make these biofuels from biomass feedstock is one of the main tasks. One of the promising benefits of biomass is the cycle of capture and release of carbon dioxide, resulting in a carbon-neutral system, if the energy required for the process to be created is discounted (Figure 3).
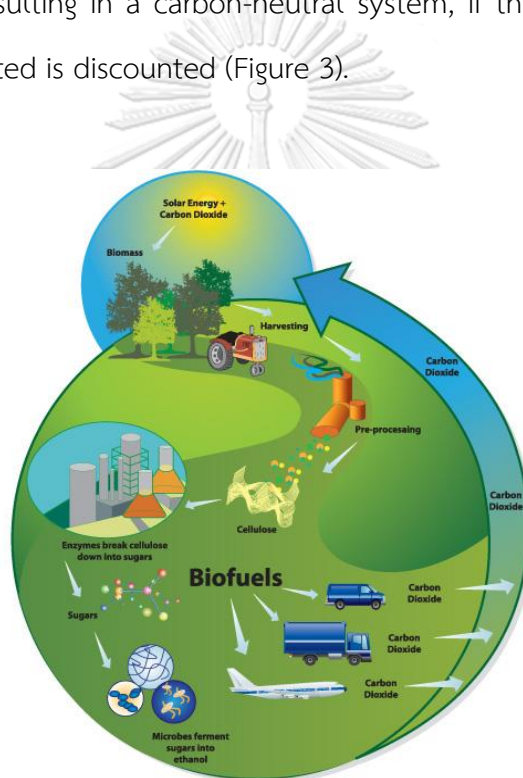
Figure 3 Biomass to biofuel cycle [7].

As alternative biofuel, 2,5-dimethylfuran (DMF) shows several of attractive properties (Table 1), such as mass density, the lower heating value, boiling point, octane rating and water solubility. The high mass density of DMF (0.88 kg·L^{-1} at 25 °C) makes the lower hating value of DMF (29.3 MJ·L^{-1}) close to gasoline (31.9 MJ·L^{-1}) leading to improve the vehicle mileage [8, 9]. DMF is higher boiling point as compared

to ethanol, resulting it is less volatile, which is good for transportation fuel. Moreover, high octane number (RON= 119) [10] of DMF is able to resist knocking, making it reduces emission of greenhouse gas and fuel consumption leading to improve fuel economy. Additionally, DMF is insoluble in water thus it will not adsorb moisture from atmosphere. Consequently, DMF is a promising alternative biofuel, with some aspects better than that gasoline and ethanol.

Table 1 Comparison of fuel quality of gasoline, ethanol and 2,5-dimethylfuran [11].

Name	2,5-Dimethylfuran	Gasoline	Ethanol
Molecular Formula	C_6H_8O	C_2-C_{14}	C_2H_6O
Molecular Mass $(g \cdot mol^{-1})$	96.13	100-105	46.07
Water Solubility (25°C)	Insoluble	Insoluble	Highly Soluble
Relative Vapour Density	3.31	3-4	1.59
Structural formula	$(CH_3)_2C_4H_2O$	Variable	CH_3OCH_3
Type of Substance	Heterocyclic	Aliphatic hydrocarbon mixture	Acyclic
Aroma	Spicy Smokey	Petroleum odour	Vinous
Lower Heating Value $(MJ \cdot kg^{-1})$	33.7	42.9	26.9
Heat of vaporization $(kJ \cdot kg^{-1})$	332	373	840
RON	119	95	110

2.3 5-Hydroxymethylfurfural applications

5-Hydroxymethylfurfural (HMF) has an IUPAC name of 5-(hydroxymethyl)2-furaldehyde, and it contains a heteroaromatic furan ring with both reactive aldehyde and alcohol functional groups. Its molecular formula is $C_6H_6O_3$, and a few physical properties include: molecular weight of 126.11 g·mol^{-1}, building point of 112 °C, yellow solid at room temperature and dissolves in water. HMF is obtained from the acid catalyzed dehydration of lignocellulose such as sugarcane, agar and bagasse [9, 12]. HMF has been considered as a key intermediate for biomass conversion into valuable biofuel and other useful chemicals. There are several pathways and products for the HMF upgrading such as alkoxymethylfurfurals (2), 2,5-furandicarboxylic acid (3), 5-hydroxymethylfuroic acid (4), bishydroxymethylfuran (5), 2,5-dimethylfuran (6) and the diether of HMF (7) are furan derivatives with a high potential in fuel and/or polymer applications. Some important non-furanic compunds can also be produced from HMF, namely levulinic acid (8), adipic acid (9), 1,6-hexanediol (10), caprolactam (11) and caprolactone (12) as presents in Figure 4 [10, 12].
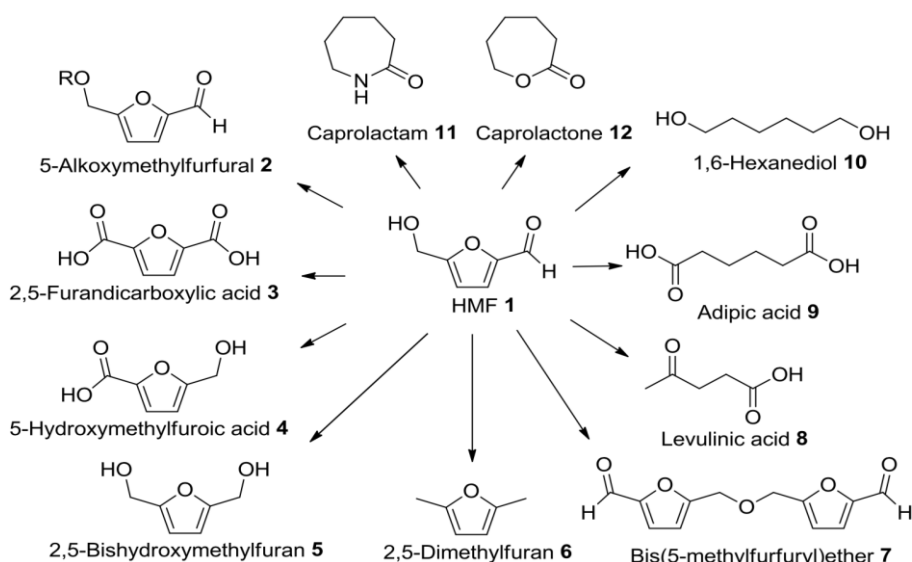
Figure 4 HMF as a platform chemical [12].

All furanics products are obtained from oxidation, hydrogenation and hydrogenolysis reaction respectively. A leading biofuel candidate, hydrogenation is still the most versatile reaction for upgrading HMF to biofuels. Hydrogenation of HMF has been used to produce DMF, which is widely used in gasoline blends and chemical industry.

2.4 Hydrogenation of 5-hydroxymethylfurfural

   The DMF production from hydrogenation and hydrogenolysis of HMF consists of two possible pathways as presents in Figure 5. Path 1, HMF is converted to DHMF by hydrogenation of C=O bond of the aldehyde group, then DMF is achieved from hydrogenolysis of CH_2-OH bonds in DHMF. Path 2 is the conversion of HMF to 5-methylfurfural (MF) through hydrogenolysis, followed by hydrogenation of MF and hydrogenolysis of 5-methyl fufuryl alcohol (MFA). Most studied reported that Path 1 is the main route for DMF production [13-15].
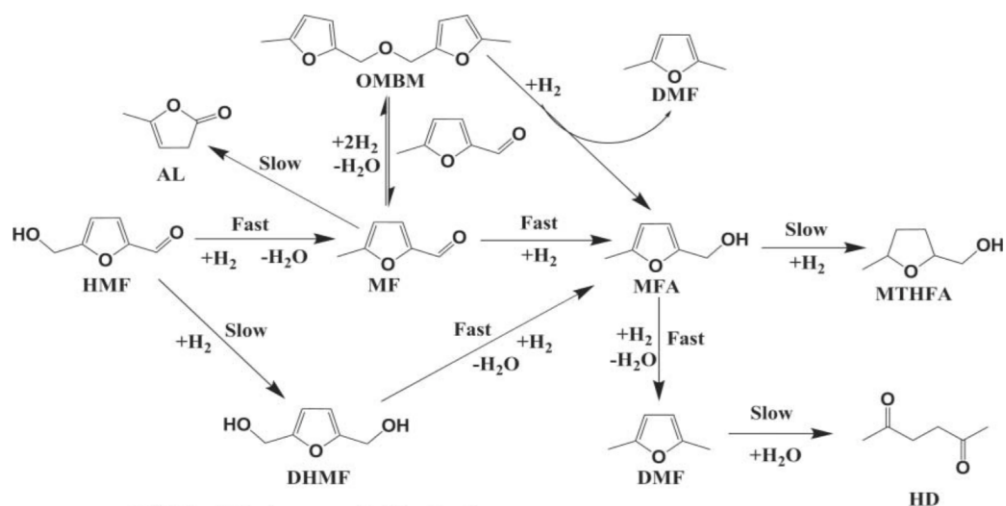
HMF = 5-hydroxymethylfurfural   MF = 5-methylfurfural

MFA = 5-methylfurfuryl alcohol   DHMF= 2,5-dihydroxymethyl furan

DMF = 2,5-dimethylfuran   MTHFA = 5-methyltetrahydrofurfuryl alcohol

HD = 2,5-hexanediene   AL = Angelicalactonec

OMBM = 5,5-(oxybis(methylene)bis(2-methylfuran))

Figure 5 Reaction pathway for DMF production from HMF [14].

During DMF production, there are many competitive pathways such as partial hydrogenation, total hydrogenation, ring hydrogenation, ring opening and hydrodeoxygenation that provide a variety of chemicals such as 2,5-di(hydroxymethyl)furan, 5-methylfurfural, 5-methylfurfuryl alcohol, 2,5-dimethylfuran, 2,5-di(methyl)tetrahydrofuran and others, which depends on the reaction conditions (temperature and pressure), hydrogen sources (molecular hydrogen, formic acid and alcohol) and the catalyst employed. Typically, the HMF hydrogenation was carried out in the temperature range of 120 and 300 °C. Noble-based catalysts (Pd, Ru, Pt) were most used, and many studies were performed in batch reactor [16, 17]. The possible products of HMF hydrogenation are presented in Figure 5. Moreover, the hydrogenation of HMF could be carried out in the liquid and vapor phase. The vapor phase was widely used owing to requirement for catalyst regeneration. The catalyst recovery in the vapor phase is facilitate an economical process, which is positive effect for the environment. Currently, liquid phase was also employed for hydrogenation of HMF because it needs lower temperature in comparison with vapor phase, leading to energy saving [10, 18, 19].

2.5 Catalysts for hydrogenation of HMF

The catalysts for hydrogenation of HMF toward DMF was classified as monometallic and bimetallic catalysts.

2.5.1 Monometallic catalysts

Noble metal-based catalysts (Pd, Ru and Pt) and non-noble metal-based catalysts (Cu and Ni) have been reported for HMF hydrogenation and hydrogenolysis toward DMF.

2.5.1.1 Pd-based catalysts

Pd-based catalysts have presented high efficiency for the hydrogenation of HMF. Chatterjee *et al.* [20] explored activated carbon supported Pd catalyst for

hydrogenation and hydrogenolysis of HMF to DMF at 80 °C under 10 bar H_2 pressure at 2 h. They found that Pd/C catalyst exhibited high conversion (95%) with moderate DMF yield (42%). They explained that moderate yield of DMF was achieved because the catalyst favoured the hydrogenation of furan ring. However, when, carbon dioxide and water were introduced into the reaction system, 83 % yield of HMF was observed, suggesting due to the acidity from the combination of carbon dioxide and water. The reaction medium became acid after carbon dioxide was applied in the reaction, which could enhance the DMF product. A commercial Pd/C catalyst was found to produced high yield of DMF (85%) at 120 °C under 2 bar hydrogen pressure at 15 h reaction time with the adding of formic acid and acetic acid into the reaction system [21]. Interestingly, as the weak acid was introduced into the reaction, a high yield of DMF was observed under lower hydrogen pressure. The weak acid liked as hydrogen source, which was activated to hydrogenolysis and suppressed decarbonylation and hydrogenation of furan ring [21]. Although the addition of acid could enhance a high yield of DMF, which could produce a large amount of waste and the corrosion of the reactor system. Gawked *et al.* [22] solved this problem, they prepared metal-acid bifunctional catalyst, 2%Pd-20%Cs dodeca-tungstophosphoric acid supported on K-10 acidic clay. The catalyst provided high performance for hydrogenation and hydrogenolysis of HMF to DMF in tetrahydrofuran as solvent, and the catalyst presented similar results to the combination of 5% Pd/C and HCl. This study indicated that acidity of clay support played an important role to obtain high both conversion (98%) and DMF selectivity (81%) at 10 bar of hydrogen pressure and 90 °C for 2 h. For this catalyst, the acidic K-10 clay catalyzed the hydrogenolysis of hydroxy group of 2,5-dihydroxymethylfuran (DHMF) while Pd sites activated the hydrogenation reaction of HMF.

2.5.1.2 Ru-based catalysts

Ru is also suitable catalysts for hydrogenation and hydrogenolysis of HMF toward DMF. Jae *et al.* [23] and Priecel *et al.* [24] investigated the hydrogenation of HMF over Ru/C and Ru/CNTs catalysts. They found that the catalysts exhibited high efficiency for the reaction, 81% and 83 % DMF yield with over 97% HMF conversion were obtained at 190 °C for 2h and 200 °C for 2h, respectively. Moreover, the catalysts revealed excellent stability for recycling test [24]. They explained that carbon supports especially CNTs were important for hydrogenolysis of HMF that probably because of electrical conductivity, which could increase the charge density of ruthenium catalysts. Additionally, Ru-based catalysts [25-27] were studied in batch experimental system. They found that Ru-based catalysts was generally high activity for hydrogenation. Although the Ru-based catalysts displayed moderate hydrogenation of C=O group as Ru has wide d band that could enhance the hydrogenolysis of HMF to DMF, it was high activity for hydrogenation of furan ring or ring opening of furan leaded to produce some by products. Hence, Ru-based catalysts are an important to choose the second metals or promoters combine with its to improve the selectivity of DMF. Moreover, Nagpur *et al.* [25] prepared the mixture RuO_2 and Ru/C catalyst for hydrogenation and hydrogenolysis of HMF to DMF. They investigated the intermediate products at each step of reaction and found that DMF was achieved by 2,5-dihydroxymethylfuran (DHMF) followed by 5-mrthyl furfural alcohol (MFA). These results was good agreement with Yang *et al.* [28] that studied the hydrogenation of HMF over Ru-MoO/C catalyst. Moreover, Yang reported that the hydrogenolysis of HMF to 5-methylfurfural was obtained over only MoO/C catalyst, instead of the hydrogenation of HMF to DHMF. Therefore, for Ru catalyst, type of support and synergistic effect of Ru and second metal are an important role to enhance the catalytic performance.

2.5.1.3 Cu-based catalysts

Currently, Cu-based catalyst has been widely studied. Although copper is not high activity as comparison to noble metal-based catalysts, it is low cost and unique properties. Moreover, the modification of reaction conditions in hydrogenation of HMF such as reaction temperature, type of solvent and hydrogen pressure or the combination between Cu and second metal, good results were obtained in some studies. Roman et al. [29] prepared $CuCrO_4$ catalyst for hydrogenation of HMF to DMF. Moderate yield of DMF (61%) with total conversion were achieved at 200 ℃ in 2 h. Similarly, Cu/ZrO_2 catalyst also revealed activity for hydrogenation of HMF toward DMF and resulted in 60% of DMF yield at 200 ℃ for 2h and 15 bar of hydrogen pressure [30]. Moreover, Gao et al. [31] investigated the hydyogenolysis of HMF in different hydrogen donor (i.e., methanol, cyclohexanol and hydrogen gas) over nitrogen doped carbon (NC)-Cu/MgAlO catalyst, the results shown total HMF conversion with DMF yield at 48%, 96% and 62%, at 260 ℃ in 3h, 220 ℃ in 0.5 h and 220 ℃ in 1 h, respectively. The catalyst exhibited high yield of DMF due to the synergistic between the high dispersion of Cu and surface basic sites, which could enhance dehydrogenation of cyclohexanol and improve the hydrogenolysis of HMF. Additionally, the (NC)-Cu/MgAlO catalyst provided good recyclability due to strong interaction between support and copper. Interestingly, Gupta et al. [18] suggested that Cu-based catalyst could prevent the hydrogenation of furan ring because strong repulsion between Cu (111) surface and rural ring and led to enhance the selectivity of DMF.

2.5.1.4 Ni-based catalysts

Ni-based catalyst has received considerable attention in the recent year, due to high activity for hydrogenation as comparison to Fe-based and Co-based catalysts. Many studies chose Ni-based catalyst for hydrogenation and hydrogenolysis of HMF to DMF. Kong, X. et al. [32] synthesiszed Ni/SIO_2 catalysts for hydrogenation of HMF.

The Ni/SiO$_2$ revealed an efficient hydrogenolysis of HMF to DMF and 2,5-dimethyltetrahydrofuran (DMTHF) at the temperature range of 130-150 °C. Similarly, a high yield of 2,5-di(hydroxymethyl)tetrahydrofuran (DHMTHF), DMF and DMTHF (over 90%) was obtained for the hydrogenation and hydrogenolysis of HMF over Ni/Al$_2$O$_3$ catalyst [32]. Though Ni-based catalysts provided high activity, it could not avoid further hydrogenation of furan ring. Additionally, various carbon supports were used for Ni-based catalysts such as Ni/C [33], 7%Ni-30%W2C/AC [34]. High yield of of DMF (75%) was achieved for that catalysts, however; the catalyst required high hydrogen pressure (over 45 bar). Moreover, this study showed that DHMF was obtained from hydrogenation of aldehyde group in HMF. After that, DHMF was converted to MFA and DMF, respectively, through hydrogenolysis. Step of hydrogenolysis toward DMF was fast while hydrogenation of HMF to DHMF step was slow, which was rate determining step. Moreover, many studies of Ni-based catalysts presented that Ni favours hydrogenation of C=C bond because it has a narrow d band width. Hence, the deep hydrogenation is easy to occur leading formation of some by products. This trouble could be prevented by adding the second metal/metal oxide or modifying reaction condition.

2.5.2 Bimetallic catalysts

In bimetallic catalysts, the existent of the second metal has an important promotional effect in catalyst efficiency. The presence of the second metal could probably change the electron density of active sites, or modify the geometry of active sites in the catalyst, resulting in enhancement of the catalytic activity. Moreover, the incorporation of second metal might also lead to prevent the carbon deposition on the active sites surface, which resulted in an improvement of the catalytic stability. Additionally, synergistic effect of two metals might play an

important role in the interaction of catalysts surface with substrate or product intermediates.

2.5.2.1 Pd-Cu based catalysts

Resasco *et al.* [35] studied the hydrogenation of furfural over bimetallic Pd-Cu/SiO$_2$ catalysts. They found that PdCu alloy phase in bimetallic catalyst could enhance the hydrogenation reaction of furfural to furfural alcohol and decarboxylation of furfural to furan. However, hydrogenation pathway was more favourable as comparison to decarboxylation. Moreover, increasing of reaction temperature (210 - 250 °C) resulted in the rise of fufuryl alcohol selectivity. DRIFT analysis for the C=O adsorption over bimetallic Pd-Cu/SiO$_2$ catalyst exhibited the strong η^2-(O,C) adsorption of carbonyl over Pd atom, while the η^2-(O,C) adsorption on the surface of PdCu alloy was weak. Further increasing of Cu content, the adsorption of η^1-O dominated over PdCu surface, resulting in the decreasing of decarbonylation product.

2.5.2.2 Ru-Cu based catalysts

Barta *et al.* [36] prepared bimetallic Cu-Ru-PMO (PMO: porous metal oxide) and monometallic Cu-PMO catalysts for DHMF and DMF production from HMF. They found that DMF was dominant product in both catalysts at the reaction temperature of 200 °C, however; at higher temperature, Cu-Ru-PMO catalyst exhibited higher DMF and 2,5-di(methyl)tetrahydrofuran (DMTHF) products as compared to monometallic Cu-PMO catalyst. They explained that Ru had high activity in hydrogenolysis of C-O bond, the synergistic interaction between Ru and Cu resulted in higher activity in the bimetallic Cu-Ru-PMO catalyst. Moreover, Iriondo *et al.* [30] studied hydrogenation of HMF to DMF over various Cu-based RuCuTi catalysts. They proposed that the achieved high catalytic performance of RuCuTi catalyst was due to the intrinsic properties of Ru and Cu in hydrogenolysis reaction. Furthermore, the basic support

promoted homogeneous dispersion of Ru and Cu active species to obtained higher activity and selectivity in hydrogenolysis reaction. Dumeric *et al.* [37] explored bimetallic CuRu/C catalyst for selective hydrogenation/hydrogenolysis of HMF toward DMF at 220 ℃ under batch reactor system. They reported that the bimetallic CuRu/C catalyst revealed Cu-like hydrogenolysis of C-O bond, while Ru species worked to protect the active Cu from poisoning.

Among all the catalysts, Pd-based catalyst exhibited high activity for HMF hydrogenation [14, 15, 38]. However, Pd-based catalyst provided moderate DMF selectivity because Pd is highly active for the hydrogenation of C=O groups and C=C bonds of the furan ring as well as hydrogenolysis of C-O bonds [8]. For non-noble metal catalysts, Cu and Ni showed good activity but these catalysts required high pressure and temperature. The problems found when using Ni and Cu catalyst are the rapid deactivation, caused by sintering and leaching of active metal during the reaction due to high temperatures and pressure required, leading to short catalyst life times. However, Pd-based catalysts was higher activity than those of Cu and Ni-based catalysts. Several approaches have been developed to improve DMF selectivity and suppress sintering and leaching of active metal. For example, the addition of Cu metal into Pd-based catalysts can enhanced the selectivity of DMF because Cu exhibited high selectivity for the hydrogenation of carbonyl group, leaving unreduced C=C bonds from the furan ring due to strong repulsion between the surface of Cu (111) and the furan ring [39-41]. Moreover, the combination between nobel metal (Pd and Pt) and second metal (Cu, Ni, Co) can enhanced the metal dispersion and interaction between active metal and catalyst support leading to inhibit sintering and leaching of active sites [28, 42].

2.6 Reduced graphene oxide as catalyst support

Carbon materials such as carbon nanotube (CNTs), carbon nanofiber (CNF) or activated carbon have been widely used as catalyst support for transition metal due to good conductive properties and large surface area [43-45].
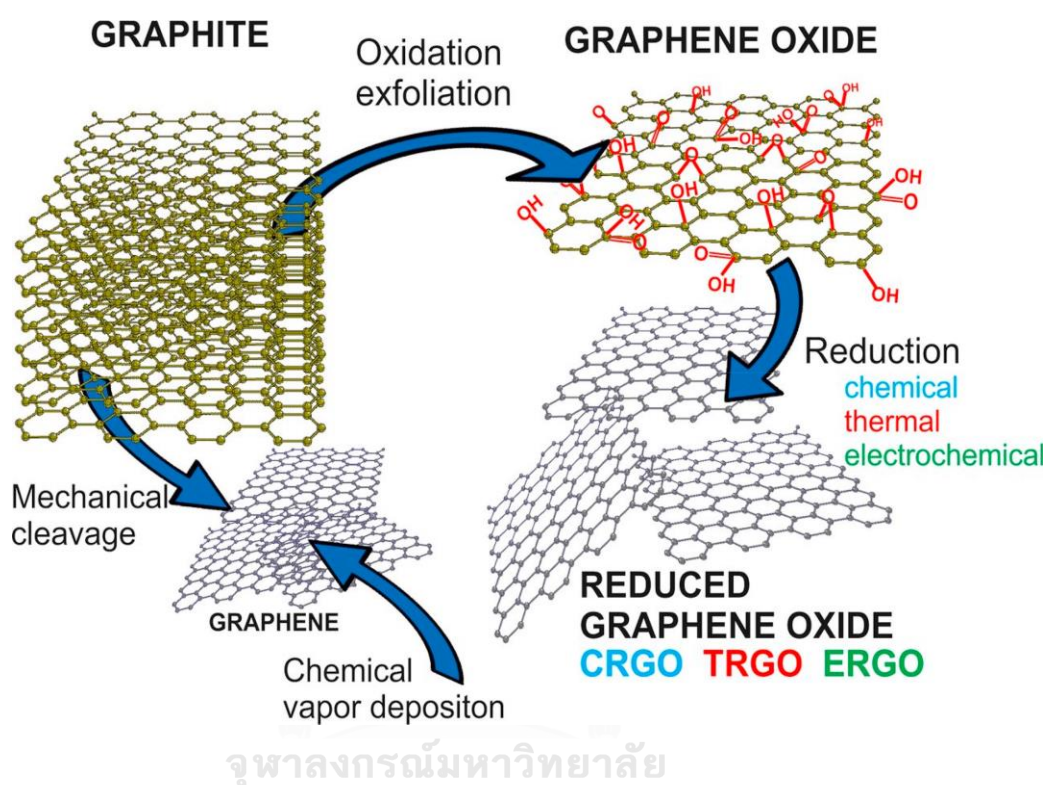
Figure 6 Possible ways for preparation of graphene and RGO [46].

Recently, graphene and reduced graphene oxide (RGO) have attracted in the attention of researchers in the world. These two dimensions sheet reveals excellent mechanical, electrical and thermal properties. These advantage, reduced graphene oxide could be used as promising for potential application in various fields [47, 48]. Moreover, the textural properties of reduced graphene oxide, it has two surfaces available for deposition of active metal transition, while the internal surface of carbon nanotube and carbon nanofiber is probably not accessible for catalyst deposition. Additionally, reduced graphene oxide contains more defects than

graphene, which produced directly from graphite [49]. The defects in reduced graphene oxide might efficiently incorporate active metal nanoparticle, and they are also useful to prevent the agglomeration of active metals, therefore; leading to form small particle size with highly dispersion. When the support characteristics including, the high specific surface area, the metal dispersion properties and thermal stability are combined, it could provide superior characteristics of catalysts support. Furthermore, non-porous support of reduced graphene oxide could also reduce diffusion limitations of reactant and products.

In general, reduced graphene oxide could be obtained by chemical, thermal or electrical reduction process, which was involving the removal of oxygen in graphene oxide such as carbonyl (C=O), carboxyl (COOH), epoxy (C-O), and hydroxyl (OH) groups [49]. The possible way for preparation graphene and reduced graphene oxide are presented in Figure 6.

2.7 Continuous-flow process

The continuous-flow process is an important for the conversion of biomass-derived platform molecules into valuable products to control reactivity. Continuous flow system has many advantages as compared to traditional batch system including faster, do not require catalyst separation after reaction (if required, it is rapidly performed), more controllable setup to maximize and fine-tune the activity and selectivity to target products and easier scale-up of the reaction conditions [50, 51], which is vital point because most processes are in the lab scale. Moreover, other advantages have been reported such lower energy consumption, high productivity and avoid the separation [52]. Thus, continuous-flow system may propose an attractive process for valorization of biomass and the study of the catalysts under certain conditions, which may occur including the presence of pressure and temperature.

Most studies for hydrogenation of furanic compounds such as furfural or HMF were carried out in batch and semi-batch experimental systems [18]. Recently, Wang *et al.* [50] explored the catalytic behavior for hydrogenation of furfural to furfuryl alcohol over monometallic and bimetallic nickel catalysts supported on activated carbon under batch and continuous flow reactors. They found that the catalyst exhibited high conversion (over 95%) at 260 °C and 30 bar hydrogen pressure in both batch and continuous flow reactors, however; low catalytic stability was obtained in continuous flow system. Which was due to active metal leaching during the reaction. Similarly, Prinsen *et al.* [53] prepared monometallic Pd, Pt, Cu and Ni catalysts supported on activated carbon (AC) for liquid-phase hydrogenation of furfural under continuous flow system. The Pt/AC catalyst exhibited the best catalytic performance as compared to other catalysts. However, the main cause of catalyst deactivation was metal leaching.

2.8 Related literatures

Zhang *et al.* [54] studied catalytic *in-situ* hydrogenation of HMF to DMF over Cu-based catalysts at the temperature range of 220-260 °C. As the results, complete HMF conversion over Cu/ZnO catalyst at 260 °C was achieved with DMF yield of 75%, suggesting that the use of Cu-based catalysts could enhanced the DMF yield.

Gao *et al.* [31] prepared nitrogen-doped carbon (NC)-decorated Cu-based catalyst for hydrogenation of HMF to DMF using cyclohexanol as hydrogen donor. The total HMF conversion and DMF selectivity of 96% at 220 °C over NC-Cu/MgAlO was achieved. They found that the present of basic sites on the catalyst could enhance the activation of hydroxyl group of cyclohexanol and then provide active hydrogen.

Lesiak *et al.* [15] developed the Pd-Cu/Al_2O_3 bimetallic catalysts to convert furfural to furfuryl alcohol under batch condition. The results showed that the addition of Cu into Pd catalysts slightly increased the catalytic activity. Meanwhile,

the selectivity of furfuryl alcohol significantly increased as compared to monometallic catalysts. They explained that the formation of palladium-copper alloy could inhibit the hydrogenation of furan ring. Moreover, the content of copper had significantly effect on the selectivity of furfuryl alcohol. Higher furfuryl alcohol selectivity (56%) was obtained over 5%Pd-6%Cu/Al_2O_3, while the decrease in copper content resulted in the lower furfuryl alcohol selectivity (48% for 5%Pd-3%Cu/ Al_2O_3 and 41% for 5%Pd-1.5%Cu/ Al_2O_3) at 90 °C and 20 bar of hydrogen pressure. Since Cu could prevent the hydrogenation of furan ring, thus it was suggested that the lower Cu content might deteriorate the furfuryl alcohol selectivity.

Du et al. [55] recently studied the hydrogenation of furfural over Cu-Pd/C catalyst using formic acid as hydrogen donor under batch condition. The catalyst provided the best performance at 170 °C with total furfural conversion and furfuryl alcohol selectivity of 98.1% at 6 h of reaction time. They explained that the selectivity of furfural alcohol was considerably dependent on the copper content. Palladium in Cu-Pd alloys was responsible for conversion of furfural by increasing hydrogen adsorption. While, copper could increase selectivity of furfuryl alcohol.

Nishimura et al. [56] investigated the activity of various noble-based catalysts (Pd, Pt, Ru and Au) for hydrogenation of 5-hydroxymethylfurfural (HMF) to 2,5-dimethylfuran (DMF) at 60 °C. The results that Pt, Ru and Au catalysts were inactive for DMF synthesis while Pd catalyst provided moderate DMF selectivity (66%) with excellent HMF conversion (91%). Moreover, the effect of catalyst support, carbon support provided the best performance with higher DMF selectivity as compared to acidic support such as SiO_2, β-zeolite, Amberlyst-15 and α-Al_2O_3, suggesting that BrØnsted acid sites of acidic support promoted ring opening of DMF by hydrolytic cleavage of furanic C-O bond.

Fulignati et al. [57] reported hydrogenation of HMF over Pt, Ru and Pd supported on carbon catalysts at 140 °C and 70 bar hydrogen pressure. Pd and Ru catalysts

exhibited higher HMF conversion as compared to Pt catalyst, suggesting that Pd and Ru could enhance the hydrodeoxygenation of HMF and ring opening, while Pt only activated the hydrogenation of HMF. However, the reaction was performed at high temperature and pressure led to disappear DMF product.

Ouyang *et al.* [58] reported the hydrogenation of furfural to furfural alcohol under continuous flow process using Pd and Pt catalysts at 90 and 150 ℃, 0.3 mL·min^{-1} of flow rate and 50 bar of hydrogen pressure in ethyl acetate. They found that the weight hourly space velocity (WHSV) and the temperature were factors that affected to the conversion of furfural and product selectivity severely. The furfural conversion and furfural alcohol selectivity at 20 min time on stream were 100% and 70%. At 480 min of time on steam, the furfural conversion decreased to 50% due to catalyst leaching during the reaction.

Garcia-Olmo *et al.* [52] studied the Pd/aluminosilicate catalyst for furfural hydrogenation in continuous flow region at 90 ℃ 0.3 mL·min^{-1} of flow rate and 50 bar of hydrogen pressure in ethyl acetate. The results exhibited moderate conversion of furfural (>60%). However, the catalyst provided a poor stability due to combining sintering and leaching of palladium catalyst.

CHAPTER III

EXPERIMENTAL

3.1. Material and reagents

The chemical materials were used in this study as listed in Table 2.

Table 2 List of chemicals and sources

Chemicals	Assay (%)	Source
Cupper acetate anhydrate ($(CH_3COO)_2Cu \cdot H_2O$)	≥ 99.0	Sigma-Aldrich
Palladium acetate ($Pd(CH_3COO)_2$)	≥ 99.9	Sigma-Aldrich
Reduced graphene oxide (RGO)	-	Nano Inova SL
Methanol	≥ 99.9	Sigma-Aldrich
Ethanol	≥ 99.9	Sigma-Aldrich
2-Propanol	≥ 99.9	Sigma-Aldrich
n-Octane	≥ 99.0	Sigma-Aldrich
5-Hydroxymethylfurfural (HMF)	≥ 98.0	Sigma-Aldrich
2,5-Dimethylfuran (DMF)	≥ 99.0	Sigma-Aldrich
2,5-Bis(hydroxymethyl)furan (BHMF)	≥ 99.0	Sigma-Aldrich
5-Methylfurfural (MF)	≥ 99.0	Sigma-Aldrich
5-Methyl furfuryl alcohol (MFA)	≥ 99.9	Sigma-Aldrich
Furfuryl alcohol (FA)	≥ 98.0	Sigma-Aldrich
2,5-Diformylfuran (DFF)	≥ 99.0	Sigma-Aldrich

3.2 Catalysts preparation

Monometallic (10Cu/RGO and 1Pd/RGO) catalysts and bimetallic (1Pd-10Cu/RGO and 2Pd-10Cu/RGO) catalysts were prepared via the wet impregnation method. $(CH_3COO)_2Cu \cdot H_2O$ (Merch, >99.5%) and $Pd(CH_3COO)_2$ (Aldrich, >99.9%) were used as metal precursor and reduced graphene oxide (RGO) as support, kindly donated by Nano Innova Technologies SL (http://www.nanoinnova.com). Typically, a certain amount of metal precursor (($CH_3COO)_2Cu \cdot H_2O$ and/or $Pd(CH_3COO)_2$) was dissolved in ethanol. Each solution was then sonicated for 10 min before its addition dropwise to a RGO suspension (1g RGO: 10 mL DI water) under stirring for 4 h. After that, ethanol was removed in a rotary evaporator. The obtained catalyst was dried at 60 °C in a vacuum oven and calcined at 500 °C for 2 h under 50 mL·min^{-1} of N_2 flow. Then, the catalyst was activated at 400 °C for 2 h under 50 mL·min^{-1} of H_2 flow. The Cu loading was fixed at 10 wt% and varying Pd loading from 1-2 wt% in the bimetallic catalyst. For monometallic catalysts, Cu and Pd metal loadings were 10 and 1 wt%, respectively.

3.3 Catalysts characterization

The catalysts were characterized by using nitrogen adsorption measurement, scanning electron microscopy-energy dispersive X-ray spectroscopy (SEM-EDX), powder X-ray diffraction (XRD), X-ray photoelectron spectroscopy (XPS), transmission electron microscopy (TEM) and temperature programmed reduction of hydrogen (H_2-TPR).

3.3.1 Nitrogen adsorption measurement

Nitrogen adsorption desorption analysis implicates the measurement the N_2 volume adsorbed on the catalyst surface at different relative pressure. The shape of N_2 adsorption isotherm can indicate the type of catalyst structure such as mesoporous structure, which normally reveals type IV of adsorption isotherm (IUPAC

classification) that has pore diameter in the range of 2-50 nm. The specific surface area, pore diameter and pore volume can be calculated by N_2 adsorption isotherms. In this work, N_2 adsorption measurement was performed to analyze the surface area and porosity of catalysts using Micromeritics ASAP 2000 volumetric adsorption analyzer (Micromeritics Instrument Corp., GA, USA) as presents in Figure 7. Nitrogen adsorption/desorption was analyzed at -196 °C. First, the sample was pretreated at 130 °C overnight under vacuum (P<0.01 Pa). The specific surface area of catalyst was determined by using Brunauer-Emmett-Teller (BET) equation [59]:

$$\frac{p}{V(p_0-p)} = \frac{(C-1)p}{CV_mp_0} + \frac{1}{CV_m} \tag{1}$$

When: V=the volumetric uptake of N_2 at pressure P

p= Equilibrium pressure

V_m= the N_2 volumn adsorbed (monolayer) at STP

p_0 = the saturated pressure at the measured temperature

C = constant relating to the free energy of adsorption

A linear graph from BET equation is made from a plot of $\frac{p}{V(p_0-p)}$ and $\frac{p}{p_0}$, V_m is then obtained from the intercept and slope. The surface area of catalyst can be calculated with [59]:

$$S_g = 4.35 \, V_m \tag{2}$$

The Barrett-Joyner-Halenda (BJH) method was used to determine pore diameter and pore volume. The BJH theory involves the desorption of the N_2 that used the Kelvin equation to calculate the pore diameter [59]:

$$\ln\frac{p}{p_0} = \frac{2\sigma V_m}{rRT} Cos\theta \tag{3}$$

Where: p = the equilibrium vapor pressure of the contained liquid in a pore

P_0= the equilibrium pressure of at a plan surface

σ = surface tension

V_m = liquid molar volume

θ = contact angle

r = pore radius

R = real gas constant

T = temperature

Figure 7 Micromeritics ASAP 2000 [60].

3.3.2 Scanning electron microscopy-energy dispersive X-ray spectroscopy (SEM-EDX)

The SEM is normally used coupled with EDX as detector, which performs to determine the metal content present in the catalyst. For the X-ray generation in SEM, first, the electron beam attacks the sample and transfers some of energy to the sample atom. The electron from the inner shell of atom obtains this energy to be knocked off from the atom, hole is then generated, resulting in electron from outer shells (higher energy shell) replaces these displaced electrons. When electron from outer shell fills the hole in inner shell, the energy difference between these two shells is released in form of characteristic X-ray. The characteristic X-ray is a unique of the element that can use to identify the element type [61]. Moreover, the peak

area from EDX spectra is used to calculate the weight percent of each element that presents in the sample. A diagram of component in SEM is presented in Figure 8A.

The elemental analysis of synthesized catalysts in this work was investigated by using a JEOL JSM 7800F scanning electron microscope (JEOL Ltd., Akishima, Tokio, Japón) (Figure 8B) equipped with an Inca Energy 250 microanalysis system, window detector of Si/Li type, detection range from boron to uranium, and resolution range of 137 - 5.9 keV.
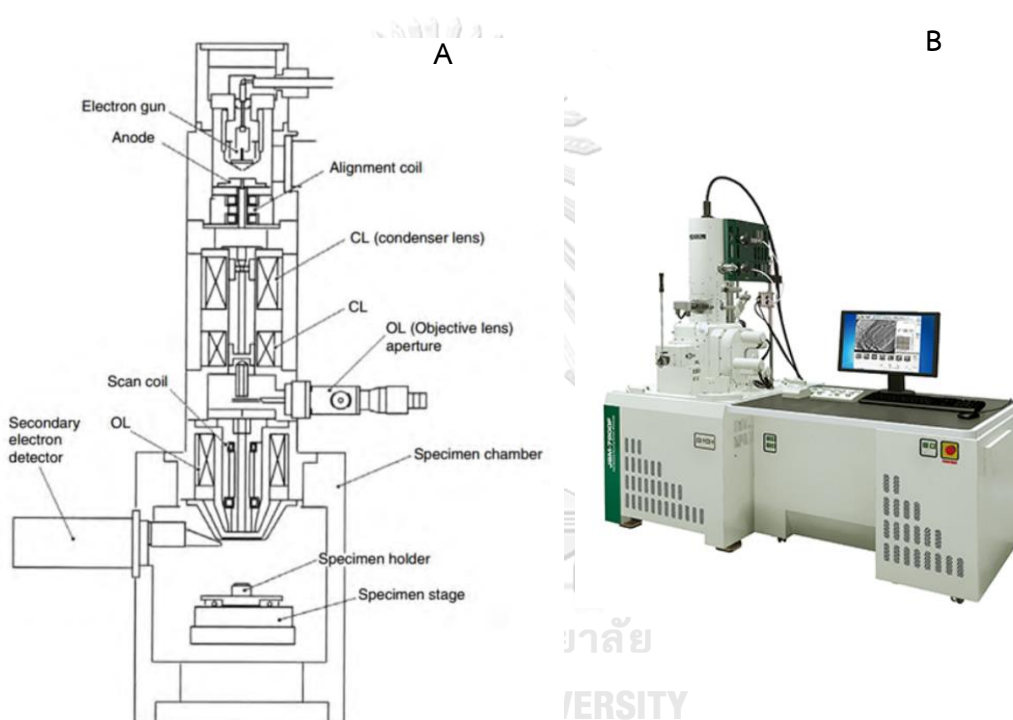
Figure 8 (A) SEM apparatus [61] and (B) JEOL JSM 7800F SEM [62].

3.3.3 Powder X-ray diffraction (XRD)

X-ray diffraction is investigated to study periodically ordered structure in atomic level. The crystal structure of sample can diffract X-ray incident on crystalline solid as see in Figure 9A. Every crystal structures have planes, a rise from repeated arrangement of atoms, which can diffract X-ray and the repetitive arrangement of atoms in crystalline structure provides the diffraction pattern. The diffraction pattern of every compound is a unique. If the sample is amorphous materials, there is no

repeating, resulting in no diffraction pattern. XRD gives data regarding the lattice structure and interplanar spacing [63]. Moreover, the crystal particle size can be determined using the Scherrer's equation (Eq.4) from evaluated width of their diffraction peaks [63].

$$B(2\theta) = \frac{K\lambda}{L Cos\theta}$$ (4)

B = average crystalline size

K = Scherrer constant (0.87-1.0, normally taken to be 1.0)

λ = the wavelength of the X-ray (1.5418 Å)

L = the breadth of a reflection in radians 2θ (FWHM)

This work, powder X-ray diffraction measurements were performed to examine the crystal structure and cluster size of catalysts at room temperature by using Bruker D8-Advanced Diffractometer (Figure 9B) with Cu-K$_\alpha$ radiation and operating at 40kV and 40 mA. The XRD profile was scaned in the range of 10-80° with 0.02° step size at 20 s of counting time per step. The average cluster size of Cu^0, Pd^0 and PdCu$_3$ alloy were estimated by using the Scherrer's equation.
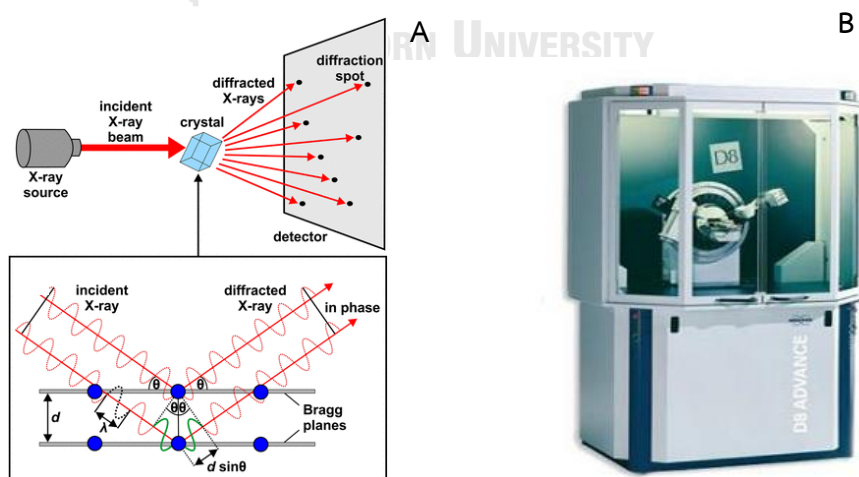
Figure 9 (A) crystalline diffraction [64] and (B) Bruker D8-Advanced diffractometer [65]

3.3.4 X-ray photoelectron spectroscopy (XPS)

XPS technique is surface analysis that presents both chemical state and elemental data. The catalyst surface is irradiated with photons from X-rays (Al-K$_\alpha$ or Mg-K$_\alpha$ source). If the interaction between electron of atom in the catalyst surface and photons from X-ray (having energy, hv) leads to photoionization, and photoelectrons are then emitted from the catalyst surface. The kinetic energy of emitted photoelectrons is [66]:

$$E_k = hv - E_b - \Phi \tag{5}$$

When E_b is the photoelectron binding energy, and Φ is the work function of spectrometer. The position of binding energy spectra can identify the elements in the catalyst surface, and the intensity peaks provides quantitative information. The oxidation state of atom changes the binding energy of the emitted photoelectron, resulting in a change of the kinetic energy [66]. The instrument is presented in Figure 10A, which includes X-ray proton source, energy analyzer and detector. This instrument is connected with computer and electronic control for information acquisition.

XPS measurements were performed to investigate the surface compositions and oxidation states of palladium and cupper on the surface of reduced catalysts for this research by using an ultrahigh vacuum (UHV) multipurpose surface analysis system Specs^{TM} with the Phoibos 150-MCD energy detector (Figure 10B). The experiments was analyzed at pressures lower 10^{-10} mbar by using a conventional X-ray source (XR-50, Specs (Berlin, Germany), Mg-K$_\alpha$, hv = 1253.6 eV, 1 eV = 1.603 x 10^{-19} J) in a "stop and go " mode. The deconvolution curves and quantification of the components were obtained by using the XPS CASA program (Casa Software Ltd., Cheshire, UK).

A   B
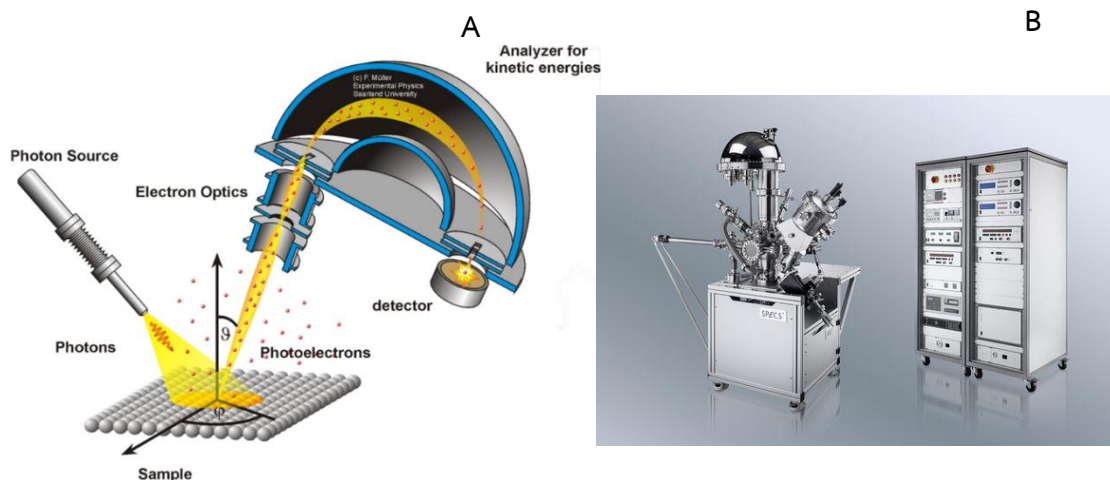
Figure 10 (A) XPS apparatus [67] and (B) ultrahigh vacuum (UHV) multipurpose surface analysis system Specs^{TM} [68].

3.3.5 Transmission electron microscopy (TEM)

TEM works on the same principle of light micrograph, but it uses electrons replace the use of light. Electrons are used as the light source in TEM analysis, and the electron wavelength is lower than that of light, which makes it to obtain higher resolution than a light microscope. Hence, TEM presents the best detail of morphology of catalyst or internal structure. At the top of microscope, the light source (electron gun) emits the electrons, and then, electrons are focused by electromagnetic lenses into very thin beam. The electron beam then attacks through the specimen to be studied, and some electrons are transmitted and disappeared, which depends on the density and electron transparency of the sample. The unscattered electrons hit a screen fluorescent that obtains rise to a shower image of the sample with its different portion presents in several darkness depending on their thickness. The darker area of figure presents the sample area with lower transmitted electrons as compared to lighter areas [61]. The TEM instrument is illustrated in Figure 11A.

In this work, transmission electron microscopy (TEM) micrographs were recorded in a FEI Tecnai G^2 (Figure 11B) equipped with a charge-coupled device (CCD) camera to analyzed the morphology of catalysts and distribution of metallic particle. Prior to analysis, the sample was suspended in ethanol and followed by deposition on a copper grid.
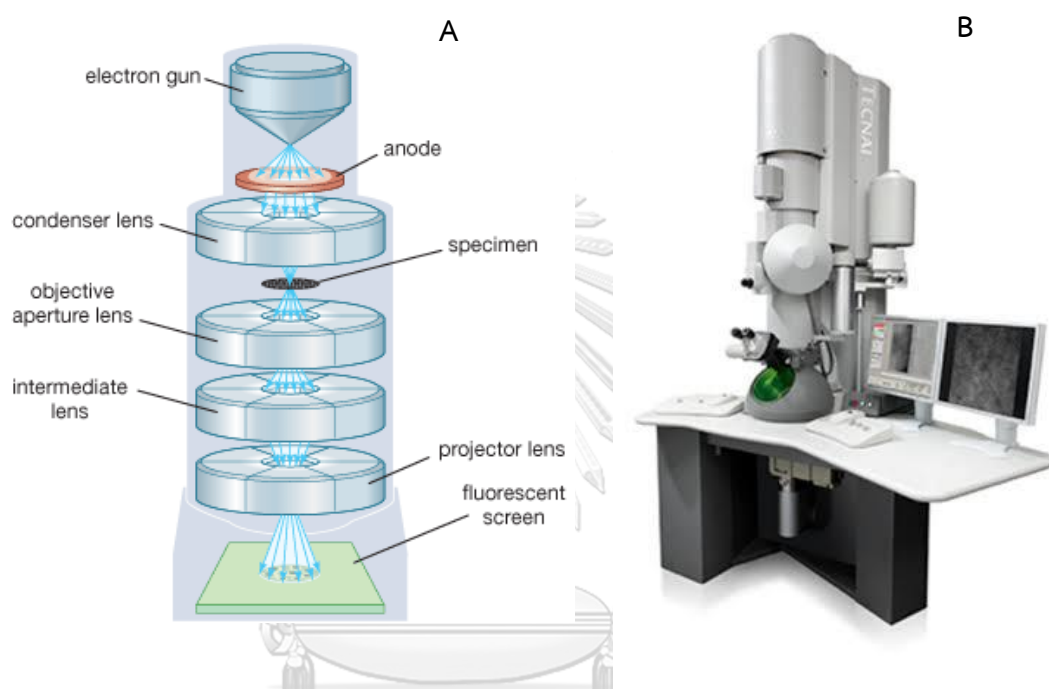
Figure 11 (A) General layout of TEM [69] and (B) TEM FEI Tecnai G^2 [70].

3.3.6 Temperature programmed reduction of hydrogen (H$_2$-TPR)

Temperature programmed reduction of hydrogen (H$_2$-TPR) was carried out to analyzed the reduction of metal oxidation. The H$_2$-TPR profiles of the catalysts were obtained with AutoChem^{TM}II 2920 (Micromeritics, USA) (Figure 12A) equipped with a thermal conductivity detector (TCD). Prior to measurement, 0.1 g of the calcinated sample was pretreated at 100 °C under argon flow at 20 mL·min^{-1} for 0.5 h. Then, the sample was cooled down to 50 °C and exposed to a reduction in 5% hydrogen in argon (5%H$_2$/Ar), while the temperature was increased up to 400 °C at the rate of 10 °C·min^{-1}. The temperature program measurement is shown in Figure 12B.
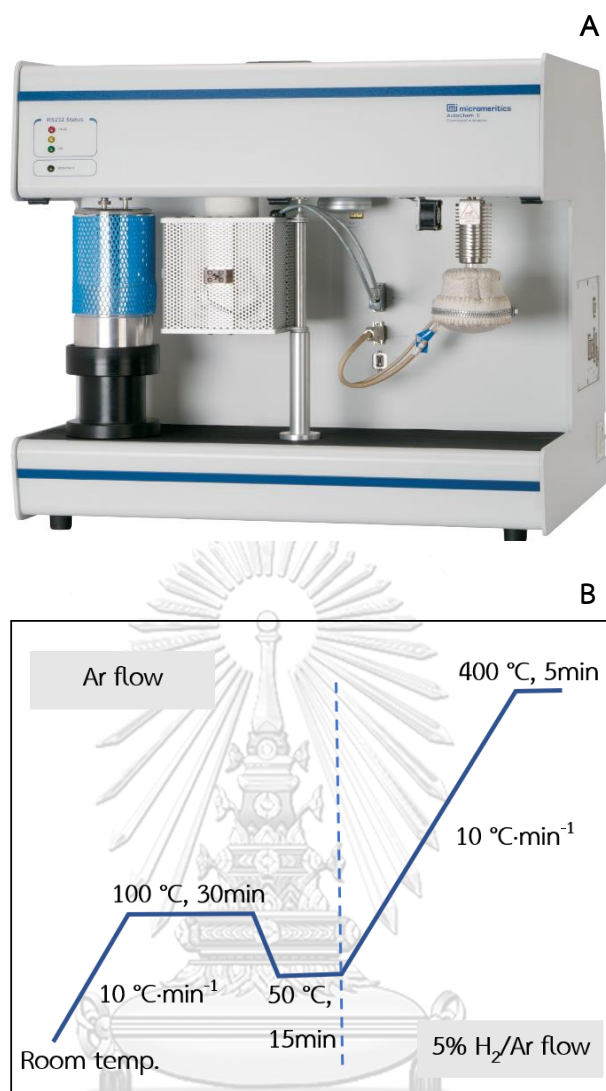
Figure 12 (A) AutoChem^{TM}II 2920 [71] and the temperature program of H$_2$-TPR.

3.4 Reaction testing

Hydrogenation of 5-hydroxymethylfurfural (Aldrich, >99%) was investigated in a Phoenix Flow Reactor (ThalesNano^{TM}, Hungary) using 2-propanol (Aldrich, >99%) as hydrogen donor. The catalyst (ca.0.11-0.12 g) was packed in 30 mm CatCart cartridge (0.88 mL empty volume) and put in the reactor module. First, 2-propanol was fed though the system using a HPLC pump before the set of temperature and pressure. When the temperature and pressure were stable, the feed stock of 0.05 M HMF in 2-propanol was pumped through. The effects of reaction temperature (140, 160, 180

and 200 ℃), feed flow rate (0.2, 0.3 and 0.5 mL·min^{-1}) and pressure (0, 15 and 30 bar) were studied. The sample at the outlet of the system was collected every 15 min until 2 h (long run 8 h) and then analyzed by GC-FID equipped with a Supelco 2-8047-U capillary HP-5 column and GC-MS (7890A)-MS (5975D inert MSD with triple-axis detector) Agilent equipped with capillary column HP-5MS (60 m × 0.32 mm). The identify products was confirmed by GC-MS.

a Pressure relative valve
b Heat exchanger
c T-valve
d Heat blocks

h=30-70 mm

Catcart

Outlet   Inlet

PHOENIX

Outlet   High pressure   Phoenix   HPLC Pump   HMF Feed
          regulator   flow reactor
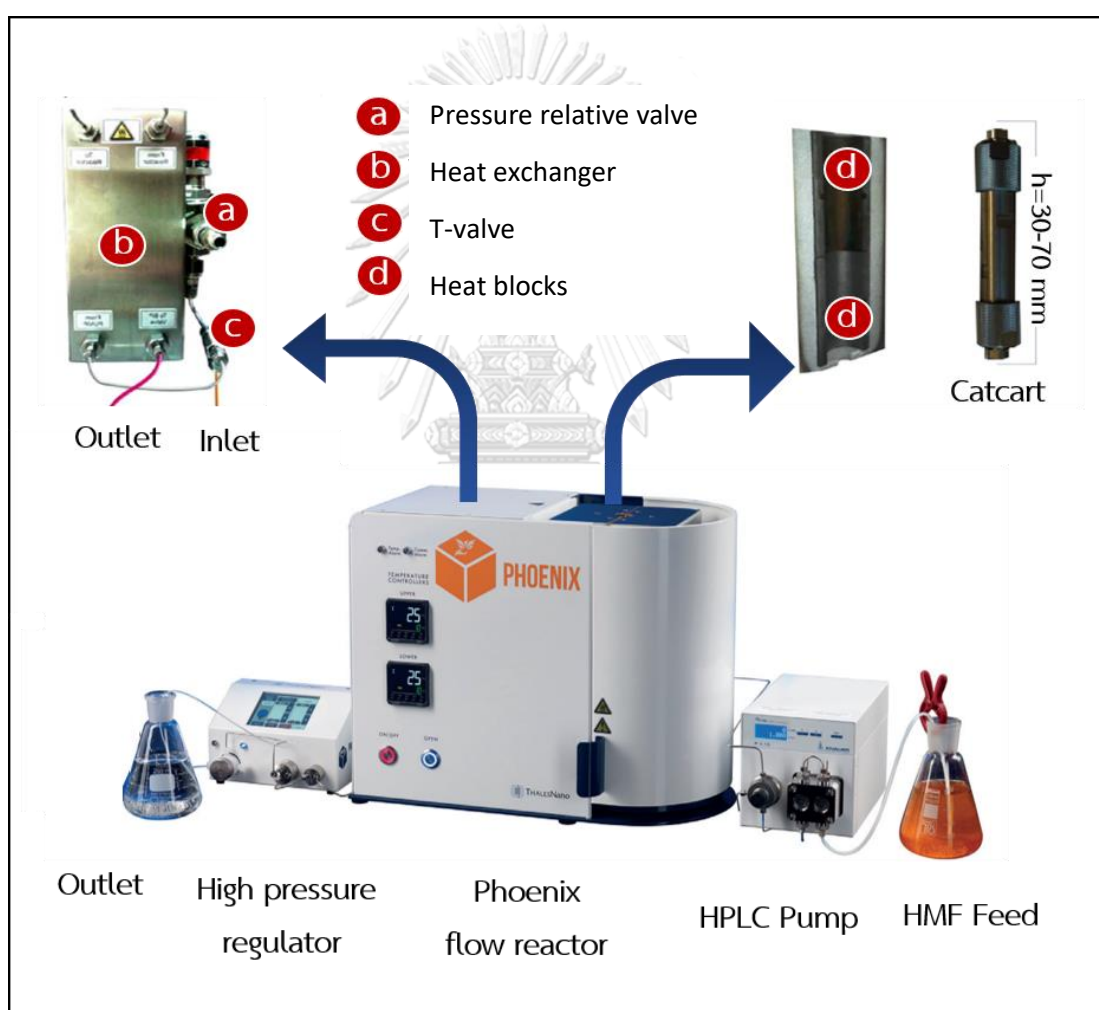
Figure 13 The Thales Nano^{TM} Phoenix equipment used for continuous flow system [72].

3.4.1 Product analysis

The product solution was detected by GC-FID equipped with a Supelco 2-8047-U capillary HP-5 column to analyzed HMF and DMF, while MF, BHMF, MFA and DMF were analyzed by using GC (7890A)-MS (5975D inert MSD with triple-axis detector) Agilent equipped with capillary column HP-5MS (60 m × 0.32 mm). The HMF and hydrogenated products were determined by using n-octane as internal standard. For GC-FID analysis, nitrogen in constant flow rate was used as carrier gas at 1 ml·min^{-1} of flow rate. The temperature of injector and detector were 280 and 300 ℃ respectively. For GC-MS analysis, the temperature of injector and detector were 300 ℃. The programmed temperature of column in Figure 14 was used to analyzed samples in both GC-FID and GC-MS. The initial temperature was 60 ℃ with 2 min of hold time, and then the temperature raised to 150 ℃ at a rate of 20 ℃·min^{-1} and held for 2 min. Finally, the temperature was ramped to 210 ℃ at 25 ℃·min^{-1} and stayed at 210 ℃ for 15 min.
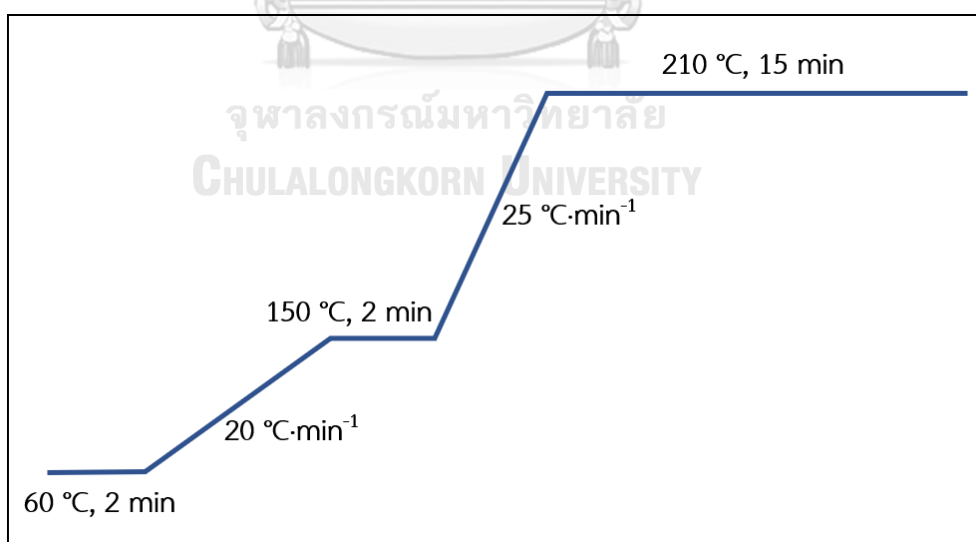
Figure 14 the GC heating programmed for gas analysis.
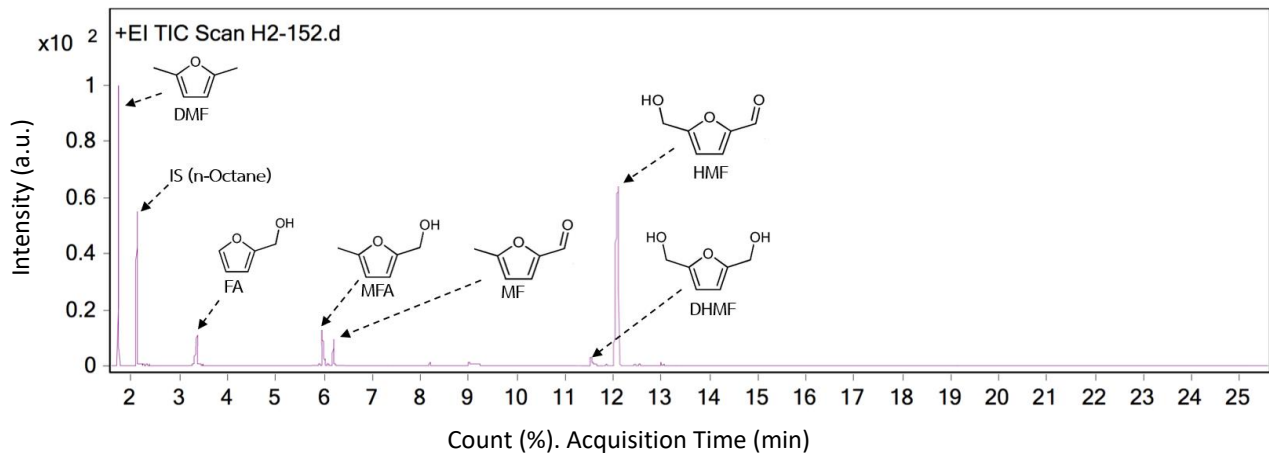
DMF = 2,5-dimethylfuran   IS = Internal standard (n-octane)

FA = furfuryl alcohol   MFA = 5-methylfurfuryl alcohol

MF = 5-methylfurfural   DHMF= 2,5-dihydroxymethyl furan

HMF = 5-hydroxymethylfurfural

Figure 15 GC-MS chromatogram of the products from hydrogenation of HMF.

The results were reported in terms of HMF conversion, selectivity and yield of each hydrogenation products, which were calculated by using eqs 6, 7, and 8, respectively:

$$X_{(HMF)} = \frac{C_{in} - C_{out}}{C_{in}} \times 100 \qquad (6)$$

When C_{in} = Molar flow rate of 5-hydroxymethylfurfural inlet (µmol·min⁻¹)

C_{out} = Molar flow rate of 5-hydroxymethylfurfural outlet (µmol·min⁻¹)

$X_{(HMF)}$ = conversion of 5-hydroxymethylfurfural (%)

$$S_{(i)} = \frac{C_i}{C_{in} - C_{out}} \times 100 \qquad (7)$$

Where C_i = Molar flow rate of the products, including DFF, DHMF, MF, MFA, FA and DMF (µmol·min⁻¹)

$S_{(i)}$ = Selectivity of products (%)

$$Y_{(i)} = \frac{X_{(HMF)} \times S_{(i)}}{100} \qquad (8)$$

When $Y_{(i)}$ = Yield of products (%)

The turnover frequency (TOF) and the weight hourly space velocity (WHSV) were calculated according to eqs 4 and 5 respectively:

$$TOF(\text{min}^{-1}) = \frac{(C_{in}-C_{out})}{\sum_0^N \frac{metal\ content}{AM} \times catalyst\ load(g)}$$ (9)

Where   AM = Atomic mass (g·mol^{-1})

$$WHSV(h^{-1}) = \frac{[HMF](Molar) \times Mw_{HMF}(g \cdot mol^{-1}) \times F(L \cdot h^{-1})}{catalyst\ mass\ (g) \times metal\ content(\%)}$$ (10)

When $[HMF]$ = Concentration of 5-hydroxymethylfurfural inlet

            Mw_{HMF} = Molecular weight of 5-hydroxymethylfurfural

            F = Feedstock flow rate

จุฬาลงกรณ์มหาวิทยาลัย

CHULALONGKORN UNIVERSITY
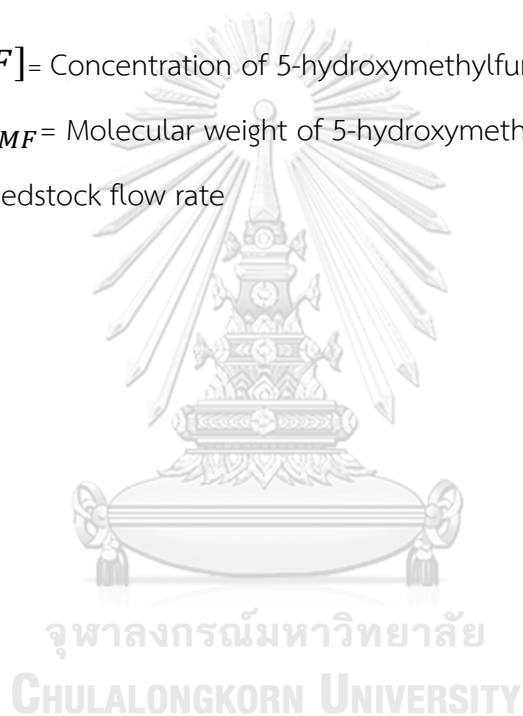
CHAPTER IV

RESULTS AND DISCUSSION

4.1. Pre-reaction catalyst characterization

Synthesized catalysts were characterized by using several techniques including BET, SEM-EDX, XRD, XPS, TEM, and H_2-TPR. The detailed characterization of all synthesized catalysts is discussed below.

4.1.1 Nitrogen adsorption-desorption measurement

Determination of textural properties was carried out as described in section 3.3.1 and nitrogen adsorption-desorption isotherms are presented in   Figure 16.
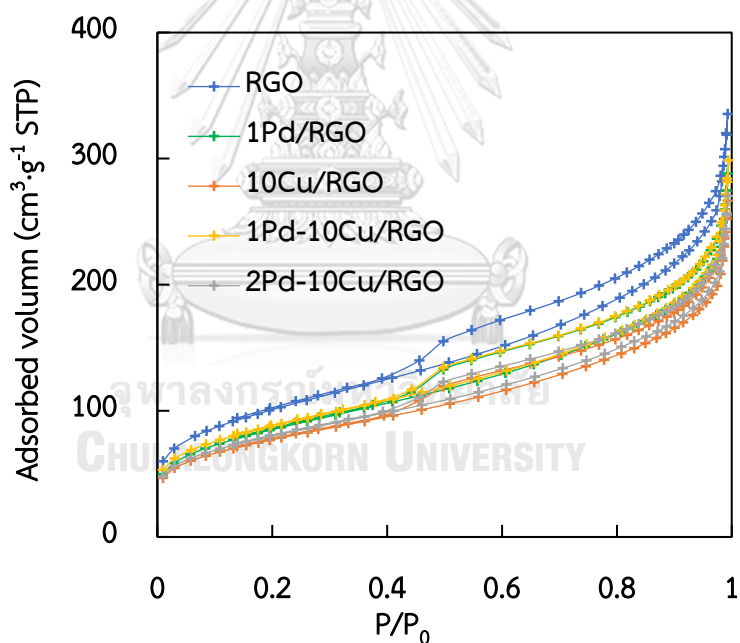
Figure 16 N_2 adsorption-desorption isotherms of RGO support and reduced catalysts.

The isotherms of support and synthesized catalysts exhibited typical type IV, according to the International Union of Pure and Applied Chemistry (IUPAC) classification, which indicated mesoporous materials [73] and the isotherms showed H_3 hysteresis loop, suggesting that slit-like pores existed between parallel layers of

graphene. Moreover, the porosity characteristics of the samples and metal content are listed in Table 3. The specific surface areas of the samples calculated by BET method ranged from 270 to 370 $m^2 \cdot g^{-1}$ while average pore sizes and pore volumes were around 5 nm and 0.5 $mL \cdot g^{-1}$, respectively. The decrease of specific surface area after metal incorporation was related to partial blockage of gaps between graphene layers. Additionally, the elemental composition was determined by SEM-EDX. The results demonstrated that Cu and Pd metal contents as analyzed by SEM-EDX was similar to the actual value.

Table 3 Textural and structural characteristics of RGO support and catalysts.

Samples	$S_{BET}{}^{a}$ ($m^2 \cdot g^{-1}$)	$D_p{}^{b}$ (nm)	$V_p{}^{c}$ ($mL \cdot g^{-1}$)	Metal content^{d} (%)		Size of Pd or Cu^{f} (nm)
				Pd	Cu	Fresh
RGO	362	5.02	0.46	-	-	-
1Pd/RGO	306	4.86	0.40	1.2	-	16
10Cu/RGO	276	4.91	0.37	-	10.8	29
1Pd-10Cu/RGO	314	4.86	0.41	0.9/0.8^{e}	10.3/7.3^{e}	19
2Pd-10Cu/RGO	286	4.86	0.36	1.7	9.7	23

^{a}S_{BET}: surface area was calculated by the Brunauer-Emmett-Teller (BET) equation.

^{b}D_p: average pore size diameter was calculated by the Barret-Joyner-Halenda (BJH) equation.

^{c}V_p: pore volumes was calculated by the Barret-Joyner-Halenda (BJH) equation.

^{d}Metal content as analyzed by SEM-EDX.

^{e}Metal content of spent catalyst as analyzed by SEM-EDX.

^{f}Crystalline size measured from Scherrer equation at (111) plan (Pd; $2\theta= 40.1$, Cu; $2\theta= 43.2$, and Cu+PdCu$_3$; $2\theta= 42.7$-43.2).

4.1.2 X-ray diffraction (XRD)

X-ray diffractometry (XRD) was performed to identify the crystalline structure by their diffraction patterns. It has been presented that the crystal with a particular set of atomic planes oriented toward the X-ray beam diffracts X-rays at an angle zeta determined by the distance between the planes. Figure 17 shows XRD patterns of RGO support, monometallic and bimetallic catalysts. The diffraction peak at 27.2° (002) in each line was attributed to diffraction peak of RGO support [73, 74]. For Pd/RGO catalyst, the diffraction peak at 40.1° was detected, corresponding to the (111) plan of metallic Pd (COD no. 1011110). The diffraction peaks corresponding to metallic Cu (COD no. 7101264) at 43.2° (111), 50.4° (200) and 74.1° (220) were observed for all Cu-based catalysts (Figure 17(A), c-e), in good agreement with previous reports [75].
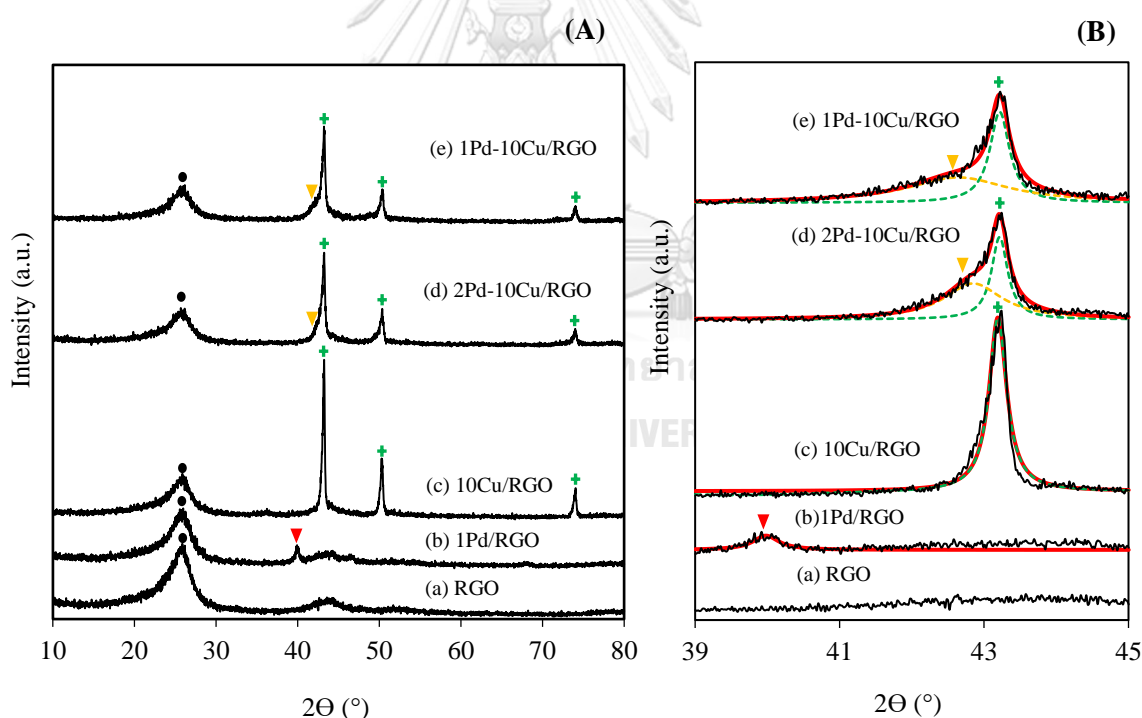
Figure 17 (A) XRD patterns of RGO and reduced catalysts and (B) the patterns after deconvolution for 2θ ranging from 39° to 45°; (a) RGO, (b) 1Pd/RGO, (c) 10Cu/RGO, (d) 2Pd-10Cu/RGO and (e) 1Pd-10Cu/RGO (symbols assignment: (●) RGO, (▼) Pd^0, (+) Cu^0 and (▼) $PdCu_3$).

Remarkably, the crystallinity of metallic copper decreased as palladium loading because the diffraction peak of Cu^0 at 43.2° overlapped with the diffraction peak of a $PdCu_3$ alloy phase. Figure 17(B) presents the patterns after deconvolution around the (111) plan of both metals (Cu^0 and Pd^0). The peak deconvolution results exhibited the overlap diffractions of metallic Cu (2θ =43.2°) and alloy phase $PdCu_3$ (2θ =42.6-42.8°) (COD no. 5910109), this result was agreement with Jiang et al. [76], and Mohammad et al. [77], suggesting the existence of a $PdCu_3$ alloy phase which could enhance Cu dispersion on the support surface. The crystallite size was determined by using the Scherrer equation using (111) diffraction line of the metals. The results are summarized in Table 3. Clearly, the bimetallic catalysts possessed better metal dispersion as compared to monometallic catalysts

4.1.3 X-ray photoelectron spectroscopy (XPS)

The surface compositions and oxidation states of palladium and copper on the surface of reduced catalysts were determined by XPS. The XPS survey spectra and the high-resolution spectra of each element including Cu, Pd, C and O of 1Pd-10Cu/RGO catalyst are presented in Figure 18. The results indicated the existence of Cu, Pd, C and O on the catalyst surface. The deconvolution of C 1s peaks (Figure 18(b)) showed the presented of four components: the C-C/C=C bond of non-oxygenated ring carbon, around 284.0 eV; the carbon in C-O-C bonds, near 285.4 eV; carbon in C=O group, around 287.4 eV; and carbon in O-C=O group, at 289.0 eV [78]. Moreover, the deconvolution of O 1s spectral is demonstrated in Figure 18(c) that contained two components at 530.5 eV and 533.1 eV, which could be ascribed to oxygen in C=O and C-O-C group, respectively [78]. The peak at 932.3 eV and 952.6 eV (Figure 18(d)), assigned to Cu $2p_{3/2}$ and Cu $2p_{1/2}$ of metallic copper [41], and Cu $2p_{3/2}$ at 934.7 eV and Cu $2p_{1/2}$ at 955.3 eV could be ascribed to Cu^{2+} [41].
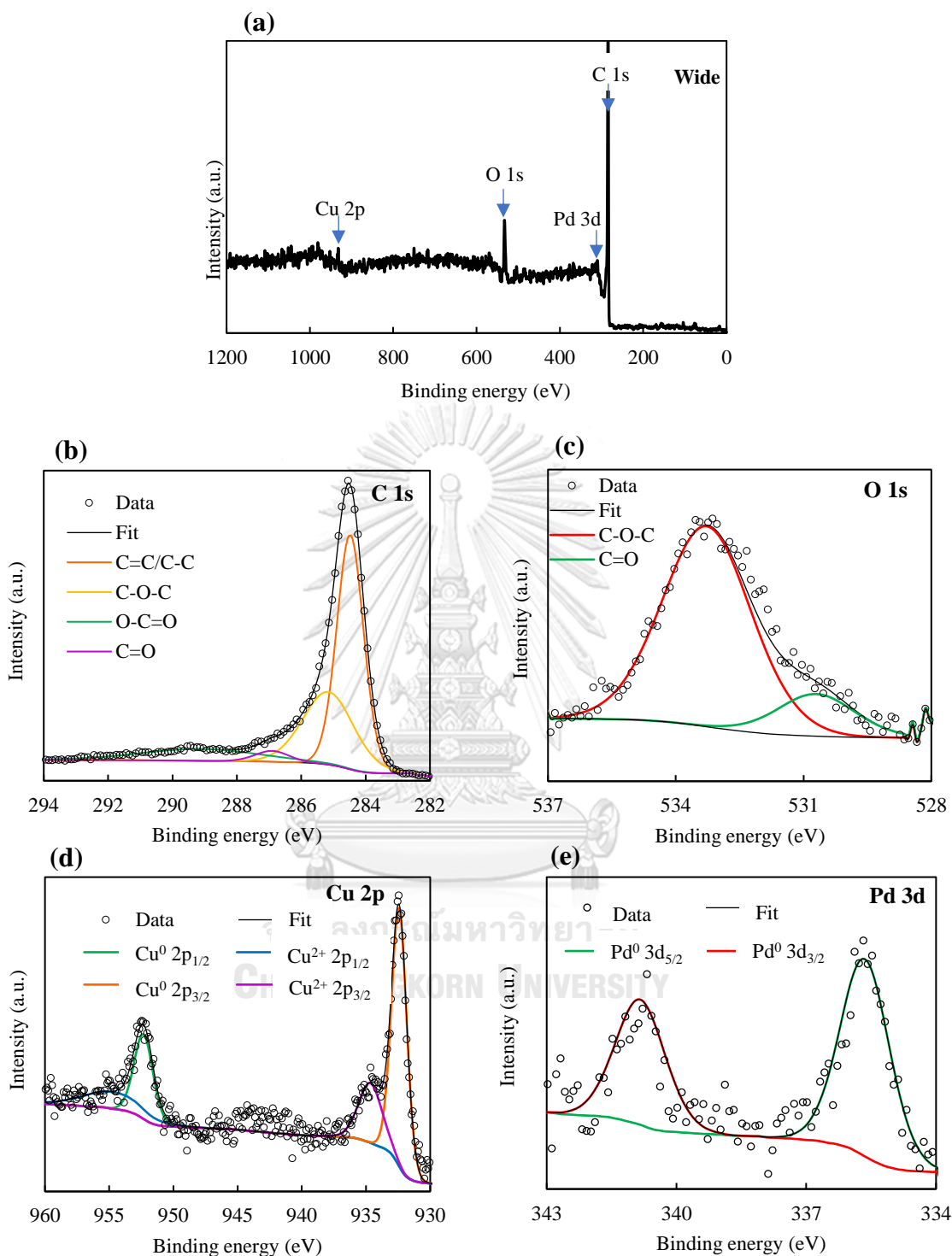
Figure 18 XPS spectra of reduced 1Pd-10Cu/RGO catalyst; (a) wide energy range survey, and high-resolution of (b) C 1s, (c) O 1s, (d) Cu 2p and (e) Pd 3d regions.

Although the Cu^{2+} species was formed on the surface due to sample transfer and keeping under air atmosphere, Cu^0 species was a major component as comparison of the area of Cu^0 and Cu^{2+} (without Cu (II) in XRD pattern). Moreover, the Pd 3d region (Figure 18(e)) showed peaks at 335.2 and 340.3 eV, corresponded to Pd^0 $3d_{5/2}$ and Pd^0 $3d_{3/2}$, respectively [75]. The XPS parameters of all catalysts are summarized in Table 4.

Table 4 XPS parameters of reduced 1Pd-10Cu/RGO catalyst

	Atomic (%)	Species	BE/eV
		C-C/C=C	284.0
C 1s	86.30	C-O-C	285.4
		C=O	287.4
		O-C=O	289.0
O 1s	10.97	C=O	530.5
		C-O-C	532.7
		Cu^0 $2p_{3/2}$	932.3
Cu 2p	2.52	Cu^{2+} $2p_{3/2}$	934.7
		Cu^0 $2p_{1/2}$	952.6
		Cu^{2+} $2p_{1/2}$	955.3
Pd 3d	0.21	Pd^0 $3d_{5/2}$	335.2
		Pd^0 $3d_{3/2}$	340.3

Figure 19 presents a comparison of Cu $2p_{3/2}$ and Pd 3d spectra of all reduced catalysts. Interestingly, the peak of Cu^0 $2p_{3/2}$ at 932.6 in 10Cu/RGO catalyst was slightly shifted to lower binding energy as incorporation of palladium (ca. 932.3 eV) as see in Figure 19A. Meanwhile, Pd^0 $3d_{5/2}$ and Pd^0 $3d_{3/2}$ peaks in 1 Pd/RGO (Figure 19B(a)) showed peaks at 335.7 and 340.8 eV, both of Pd^0 $3d_{5/2}$ and Pd^0 $3d_{3/2}$ peaks

also shifted to lower binding energy in bimetallic catalyst (335.2 eV; 1Pd-10Cu/RGO and 335.5 eV; 2Pd-10Cu/RGO). A shift of binding energy of two cases was due to the electron transfer between copper and palladium in the formation of palladium-copper alloy, in well agreement with XRD results. Fox *et al.* reported that the alloy formation induced negative peak shift around 0.1-0.4 eV [79]. The XPS parameters of all catalysts are summarized in Table 5.
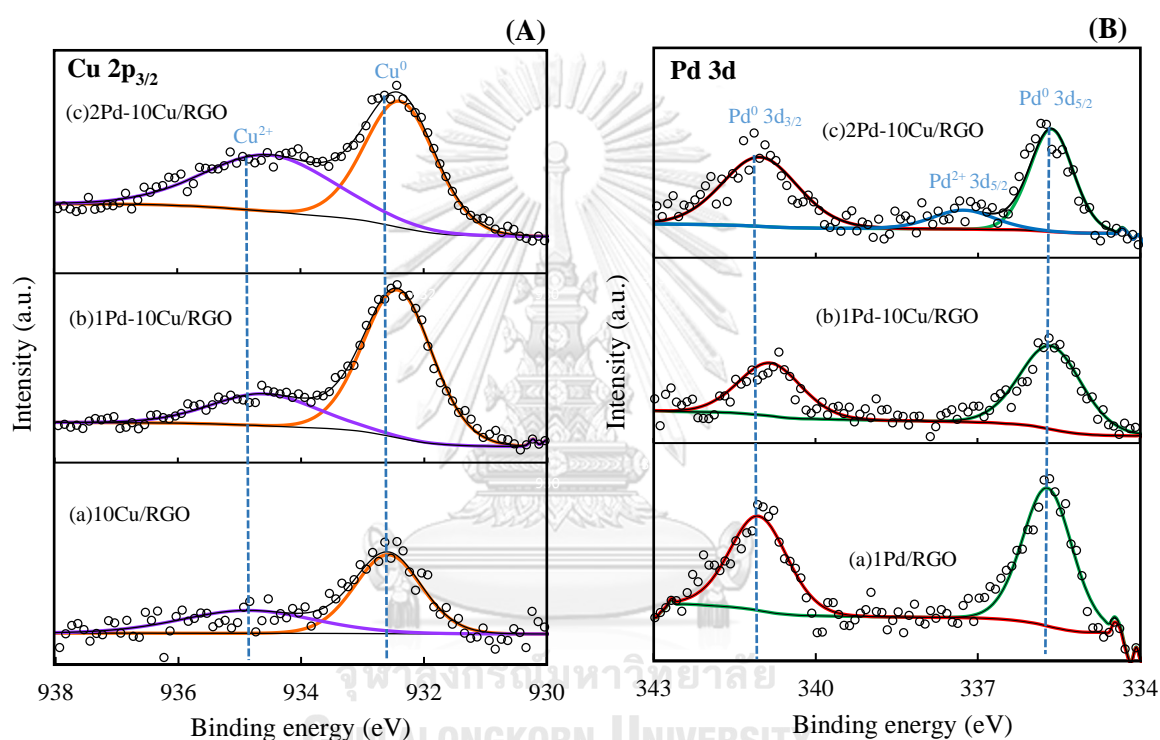
Figure 19 Deconvoluted XPS spectra of (A) Cu $2p_{3/2}$ and (B) Pd 3d states of the reduced catalysts. Reduced Cu species are likely to be related to Cu^0 but their unambiguous presence can't be disclosed from XPS results in the absence of the Auger spectra [80].

Table 5 XPS parameters of reduced catalysts

Catalysts	$Cu^0\ 2p_{3/2}$ BE/eV	$Pd^0\ 3d_{5/2}$ BE/eV	$Pd^0\ 3d_{3/2}$ BE/eV
1Pd/RGO	-	335.7	340.8
10Cu/RGO	932.6	-	-
1Pd-10Cu/RGO	932.3	335.2	340.3
2Pd-10Cu/RGO	932.3	335.5	340.5

4.1.4 Temperature programmed reduction of hydrogen (H$_2$-TPR)

The H$_2$-TPR was performed to determine the optimum reduction temperature and the reducibility of catalysts. Figure 20 displays the TPR profile of monometallic 10Cu/RGO and 1Pd/RGO catalysts and bimetallic 1Pd-10Cu/RGO catalyst after calcination. As presented in Figure 20(a), 10Cu/RGO catalyst exhibited very broad peak in the temperature of 100-300 °C. The peak deconvolution results presented two reduction peak at 148 °C and 205 °C. The first peak was assigned to the reduction of Cu^{2+} to Cu^+ and the second peak was ascribed to Cu^+ to Cu^0 [39]. Meanwhile, the 1Pd/RGO catalyst shows the reduction peak of at 78 °C, according to the reduction of Pd^{2+} to Pd^0. This result was agreement with previous report [81, 82], supported palladium catalyst was completely reduced at temperature below 100 °C and more easily reduced than the copper catalyst. In case of bimetallic 1Pd-10Cu/RGO catalyst, the reduction peak was shift to lower temperature as compared to 10Cu/RGO catalyst, indicating that the present of palladium could increase the reducibility of copper due to the formation of palladium-copper alloys. This result was in good agreement with XRD and XPS results and suggested by other reports [81, 83].
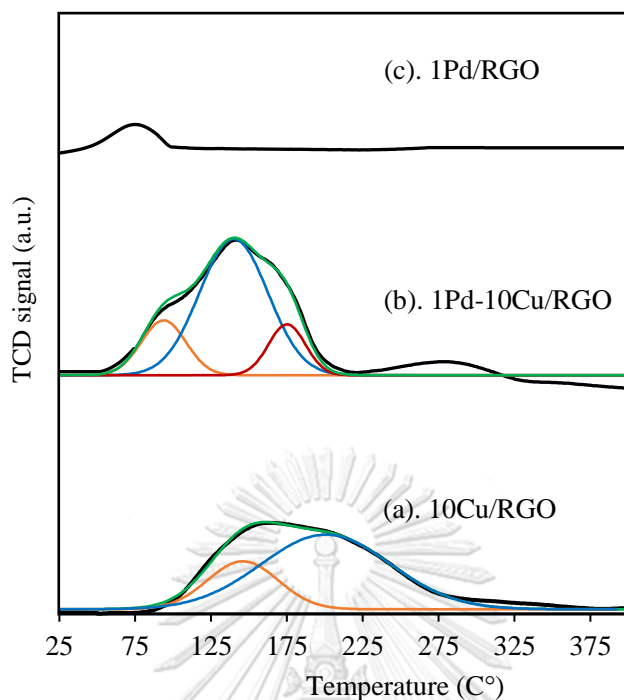
Figure 20 The H$_2$-TPR profiles of calcinated catalysts (a) 10Cu/RGO, (b) 1Pd-10Cu/RGO and (C) 1Pd/RGO.

4.1.5 Transmission electron microscopy (TEM)

TEM images were performed to study the morphology and distribution of metallic particles as displays in Figure 21. The metallic Cu and Pd were darker point, while the RGO support was lighter once. It was found that copper clusters and palladium-copper alloy were dispersed on the surface of RGO support (Figure 21B and 21C). In case of palladium-copper alloy, the 1Pd-10Cu/RGO catalyst was more homogeneously dispersed on the RGO surface than that of 10Cu/RGO catalyst, indicating that the addition of palladium element could prevent the aggregation of copper on the catalyst surface and increase the dispersion of copper particles [77]. Moreover, the particle size of metallic copper and palladium calculated from TEM micrographs was in the range of 18-28 nm, in good agreement with XRD results.
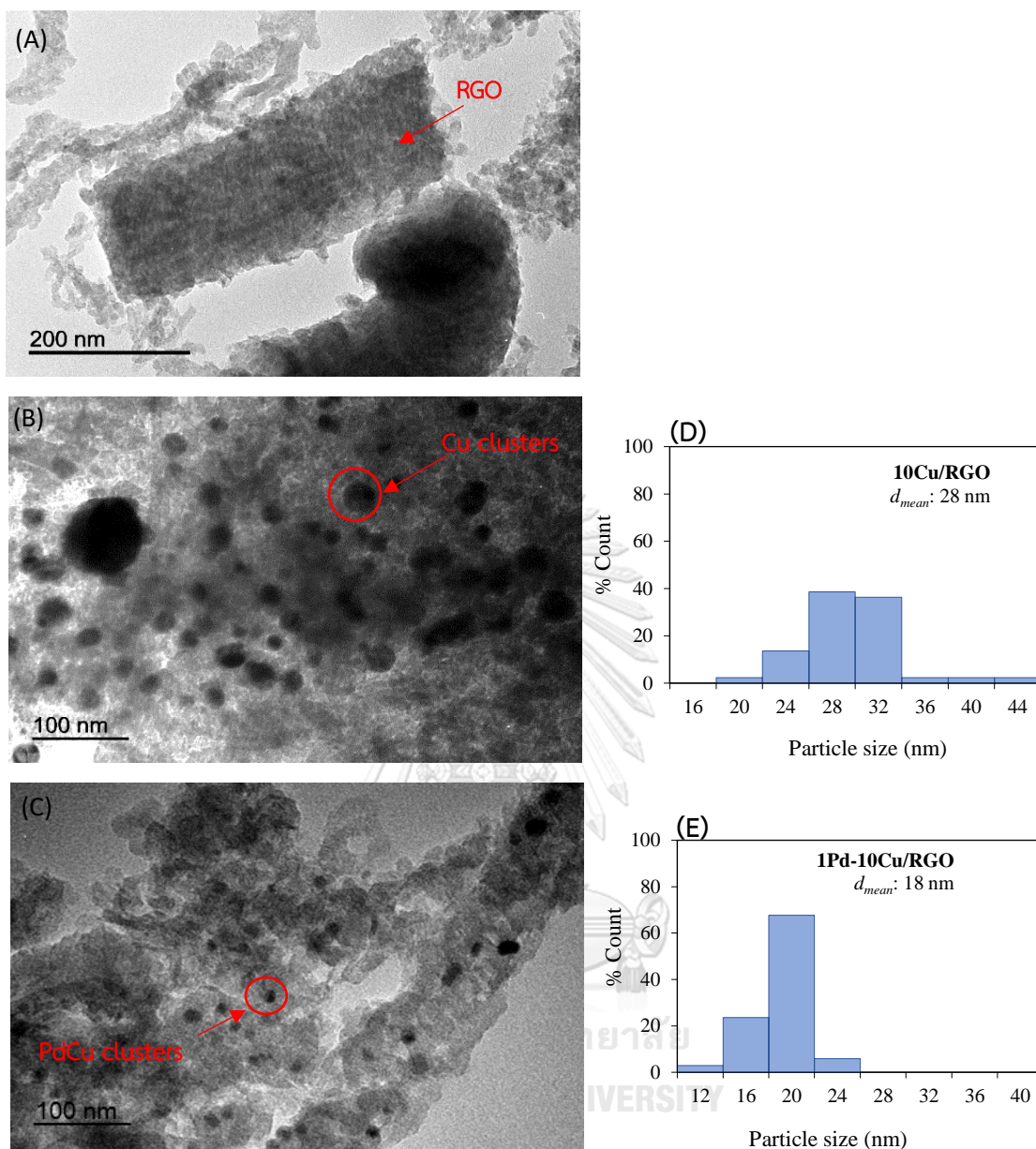
Figure 21 TEM images of (A) RGO support, (B) 10Cu/RGO and (C) 1Pd-10Cu/RGO fresh catalysts after reduction with D and E present corresponding particle size distribution.

4.2 Catalytic performance

4.2.1 Effect of different catalysts in the selective hydrogenation of HMF to DMF

Various catalysts were screened to find the best catalytic performance in the conversion of HMF to DMF under continuous flow conditions at 200 °C and 30 bar

using 2-propanol as hydrogen donor for 2 h time on stream. Catalysts performance are presented in Figure 22. For monometallic catalysts, 1Pd/RGO exhibited low activity/selectivity to DMF (28% HMF conversion and 3.9% DMF selectivity, 2 h on stream) (Figure 22B), probably due to low metal loading (ca. 1 wt%). Whereas 10Cu/RGO catalyst exhibited a good activity providing to DMF, achieving 60% conversion and 72% DMF selectivity at 30 min as shows in Figure 22C. However, with increasing time on stream, the HMF conversion and DMF selectivity decreased rapidly, while the selectivity of DHMF increased. This result indicated that catalyst deactivation reduced hydrogenolysis of DHMF to DMF. Moreover, there was no hydrogenation of furan ring or products from ring-opening over 10Cu/RGO catalyst. However, 10Cu/RGO catalyst was rapidly deactivated under flow conditions, probably due to the aggregation of active Cu as confirmed in XRD results for the spent 10Cu/RGO catalyst (Figure 27(b)). The crystalline size of spent 10Cu/RGO increased as compared to fresh catalyst from 29 to 33 nm, see in Table 6.

On the other hand, the addition of small amounts of Pd (ca. 1-2 wt.%) into Cu-based catalysts (Figure 22,(D and E)) dramatically increased the HMF conversion and DMF selectivity (ca. over 85%) as well as good stability as compared to single metal catalysts, suggesting the existence of Pd-Cu interactions in bimetallic catalyst could enhance the catalytic activity and prevent the aggregation/leaching of active Cu led to minimize catalyst deactivation, in good agreement with previous reports [41]. Moreover, the formation of side products was fully inhibited over bimetallic catalysts. Additionally, 1Pd-10Cu/RGO catalyst exhibited a higher activity as compared to 2Pd-10Cu/RGO catalyst probably due to the smaller crystalline size (see in Table 3), achieving complete conversion and over 99% DMF yield. 1Pd-10Cu/RGO catalyst was subsequently used in further optimization.
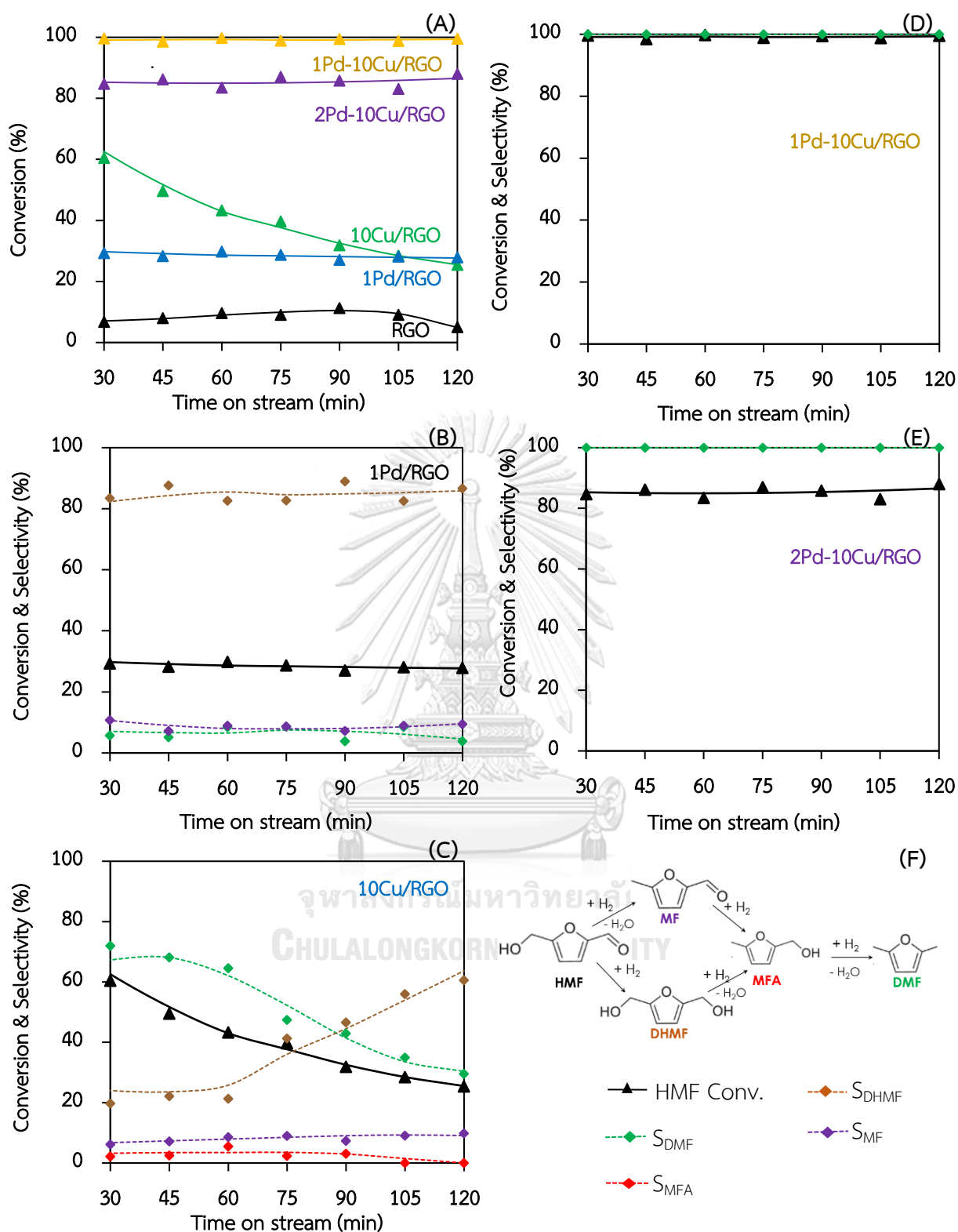
Figure 22 Effect of different catalysts on HMF hydrogenation (A) HMF conversion, (B-E) product selectivity and (F) the possible reaction pathway for hydrogenation of HMF to DMF (Reaction condition: 0.05M HMF in 2-propanol at 200 °C of temperature, 0.2 mL·min^{-1} of feed flow rate and pressure of 30 bar).

4.2.2 Effect of reaction temperature

The influence of reaction temperature on the catalytic performance of 1Pd-10Cu/RGO catalyst was studied in the range of 140-200 °C at constant reaction conditions (0.05 M HMF in 2-propanol, 0.2 mL·min⁻¹, 30 bar pressure for 2 h time on stream). The conversion of HMF as a function with time on stream is shown in Figure 23A. Above 180 °C temperature, the HMF conversion was rapidly approach to the steady state. Whereas, below 180 °C temperature, the steady state conditions were obtained after 30 min time on stream.

Figure 23 Effect of reaction temperature on catalytic performance of the 1Pd-10Cu/ RGO catalyst of (A) with TOS and (B) at 2 h TOS (Reaction conditions: 0.05M HMF in 2-propanol at 2 mL·min⁻¹ of flow rate and 30 bar of pressure).

The conversion of HMF and products distribution under steady state at 2 h time on stream are displayed in Figure 23B. At low temperatures (140 °C), HMF conversion and DMF yield were 15% and 2%, respectively, and DFF was the major

product (ca. 13%) generated *via* dehydrogenation of hydroxymethyl in HMF, indicating low hydrogenation rate at low temperatures [55]. A temperature increase to 160 °C induced mostly DMF formation with the presence of MFA, MF and FA as side products, suggesting the hydrogenation of the C=O group in HMF and DFF are favored at this temperature because of the higher activation energies of C–O and O–H .

A further increase to 180 °C rapidly improved HMF conversion from 47 to 99% at quantitative DMF yield (99% DMF). HMF conversion and DMF yield remained unchanged as the temperature up to 200 °C, indicating that the hydrogenolysis of hydroxyl group in MFA and HMF are favored at high temperatures. However, Srivastava *et al.* [84] reported that further increase in temperature resulted in over-hydrogenolysis products leading low DMF yield. Therefore, the selected optimum temperature was 180 °C for further studies.

4.2.3 Effect of feed flow rate

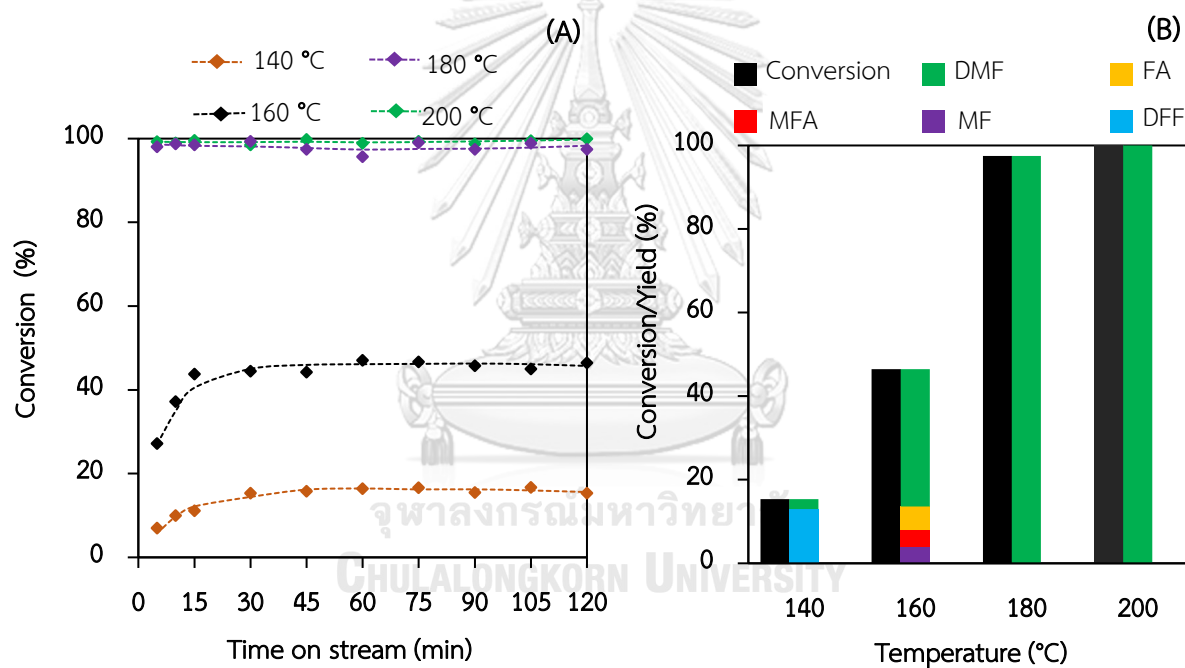*Figure 24* Effect of feed flow rate on catalytic performance of the 1Pd-10Cu/RGO catalyst of (A) with TOS and (B) at 2h TOS (Reaction conditions: 0.05M HMF in 2-propanol at 180 °C of temperature and pressure of 30 bar).

The effect of flow rate on the catalytic performance for the hydrogenation of HMF was evaluated over a flow rate range from 0.2 to 0.5 mL·min^{-1} (WHSV: 5.73-14.33 h^{-1}) using 0.05 M HMF in 2-propanol at 180 °C temperature under 30 bar pressure over 1Pd-10Cu/RGO catalyst. Figure 24A presents the results in terms of conversion with time on stream of various flow rate. Steady state conditions were obtained after 30 min time on stream at the flow rate of 0.3 and 0.5 mL·min^{-1}, while HMF conversion at 0.2 mL·min^{-1} was approached to steady state within 5 min.

Figure 24B displays the results at 2 h time on stream under steady state conditions. The HMF conversion and DMF yields decreased with an increase in flow rate. These results suggest that the contact time between reactants and active sites at high flow rate is not sufficient. Thus, the thermodynamic equilibrium of the reaction is not completed and lead to decrease catalytic activity. Hence, in order to better analyze the selective hydrogenation of HMF toward DMF, a flow rate of 0.2 mL·min^{-1} was further selected as optimum reaction condition.

4.2.4 Effect of pressure

The effect of pressure of system on HMF conversion and products distribution was investigated by varying the pressure in the systems from 1-30 bar. A set of experiments were performed by fixing the flow rate at 0.2 mL·min^{-1} using 0.05 M HMF in 2-propanol at 180 °C temperature over 1Pd-10Cu/RGO catalyst (Figure 25). The conversion of HMF was rapidly accessed to steady state at the beginning for all trials (Figure 25A).

The conversion of HMF and products distribution under steady state at 2 h time on stream are revealed in Figure 25B. Both HMF conversion and DMF yield increased upon pressure rising up to 30 bar, which provided quantitative conversion and >99% DMF yield. Interestingly, HMF conversion and DMF yield were over 95%

with 1% MFA yield as byproduct at 15 bar. Thus, 15 bar pressure was sufficient to achieve optimum yields under the investigated reaction conditions.
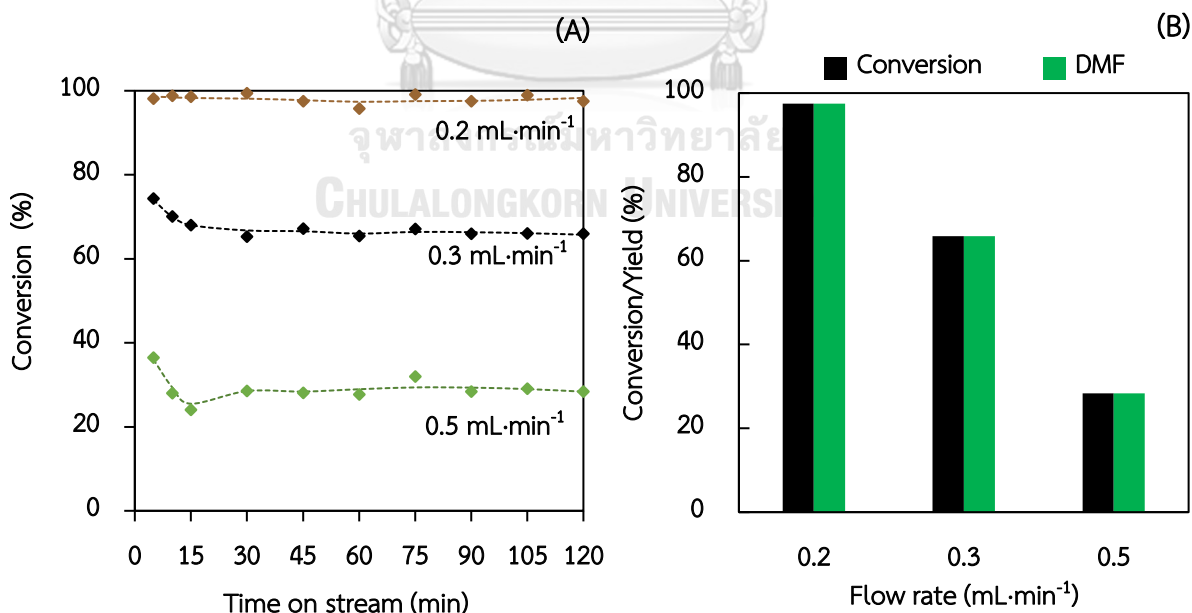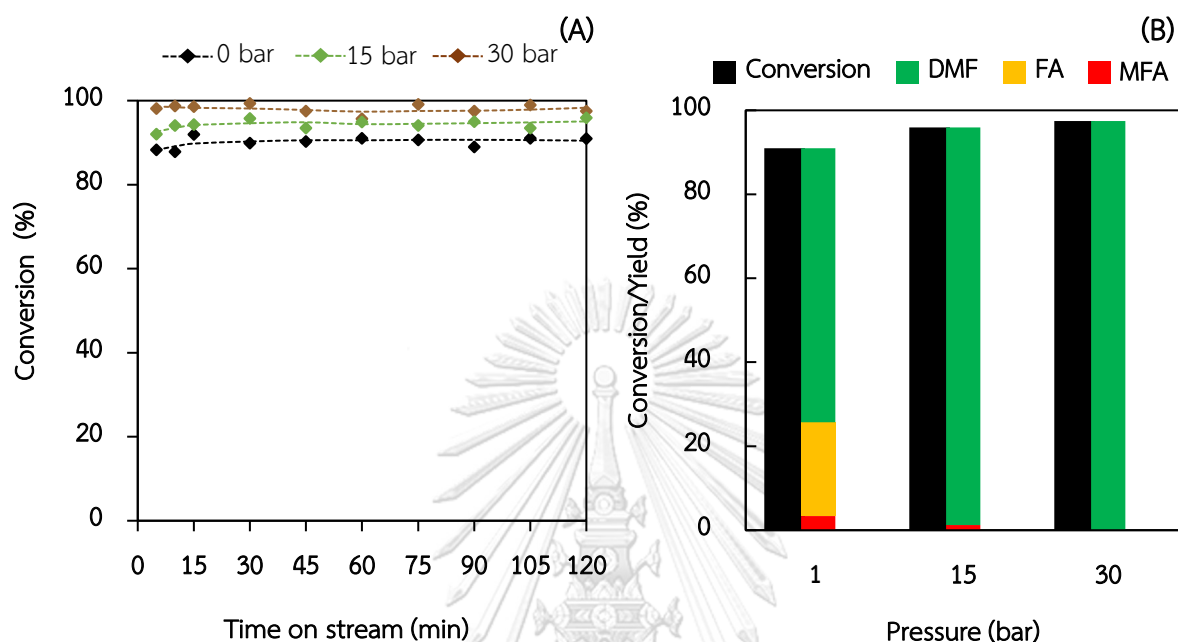

Figure 25 Effect of pressure of system on catalytic performance of the 10Cu-1Pd/RGO catalyst of (A) with TOS and (B) at 2h TOS (Reaction conditions: 0.05M HMF in 2-propanol at temperature of 180 °C and 0.2 mL·min^{-1}of feed flow rate).

4.2.5 Stability tests

Stability tests of 1Pd-10Cu/RGO catalyst was subsequently conducted at long reaction times for the selective hydrogenation of HMF to DMF over 8h time on stream at 180 °C temperature, 15 bar pressure and feed flow rate of 0.2 mL·min^{-1} (Figure 26). HMF conversion showed over 90% within 0.5 h and remained constant throughout 3.5 h time on stream. After 3.5 h, the conversion was dropped from 93 to 67% at 8 h on stream. However, the catalyst exhibited high stability in term of DMF selectivity with providing of 65% DMF yield. The decrease of catalytic performance was unequivocally due to the leaching of mostly Cu (and some Pd) in the systems

under the investigated conditions. After stability test, the copper (particularly) and palladium contents of the spent 1Pd-10Cu/RGO catalyst were found to be slightly reduced as compared to the fresh 1Pd-10Cu/RGO catalyst (see Table 3).
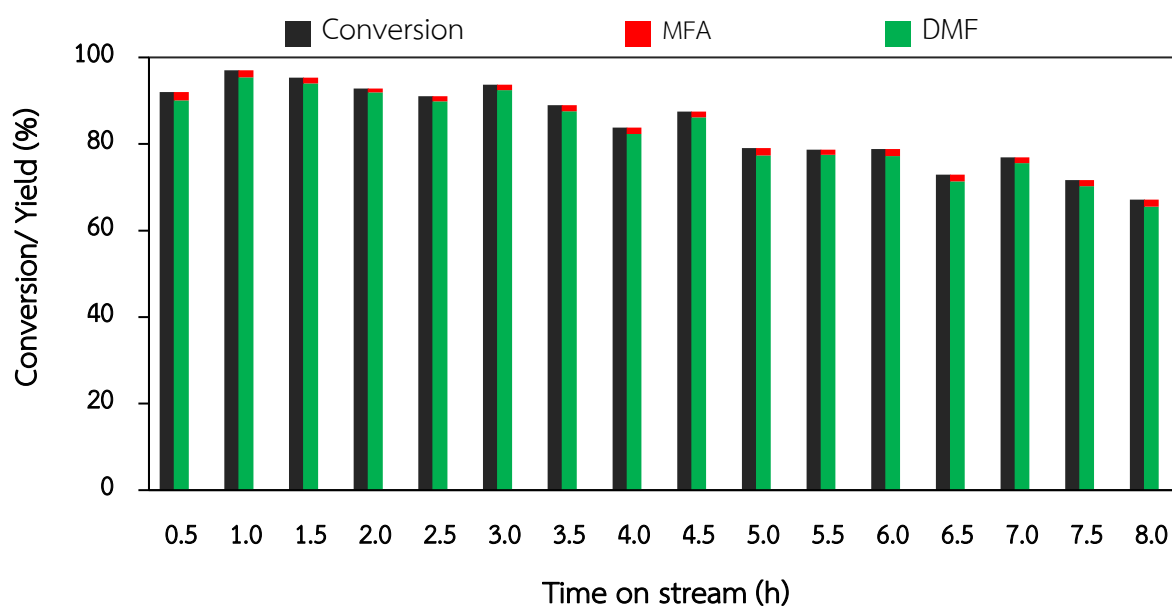
Figure 26 The stability test of 1Pd-10Cu/RGO (reaction condition: 0.05M HMF in 2-propanol, 180 °C of temperature, feed flow rat of 0.2 mL·min^{-1} and 15 bar of pressure).

4.3. Post-reaction catalyst characterization

4.3.1 X-ray diffraction (XRD)

In order to investigate the structure and metal particle size of the spent catalysts, the XRD patterns of the spent catalysts were presented in figure 27. The metallic Cu showed peaks at 2θ of 43.2° (111), 50.4° (200) and 74.1° (220) [54] for all Cu-based catalysts. The diffraction peak at 40.1° was attributed to metallic Pd [38]. In bimetallic catalysts, they displayed the diffraction peaks around 42.7° between peak

of metallic Pd and metallic Cu, which was defined as the PdCu$_3$ alloy [39, 82]. A broad peak around 23° was referred to reduced graphene oxide (RGO) [73].

Metallic particle size of Cu and Pd were calculated by using the Scherrer's equation, and the results are presented in Table 6. The crystalline size of spent 1Pd/RGO, 10Cu/RGO, 1Pd-10Cu/RGO and 2Pd-10Cu/RGO catalysts were 15 nm, 33 nm, 21 nm and 24 nm, respectively. In comparison with fresh catalysts, the crystalline size of the spent 10Cu/RGO catalyst was larger than that of the fresh 10Cu/RGO catalyst as a result from the sintering of the Cu particles. This might be another caused for the deactivation of catalyst during the hydrogenation reaction. Meanwhile, metallic crystalline size of the fresh and spent of 1Pd-10Cu/RGO and 2Pd-10Cu/RGO catalysts were rather similar, indicating that the catalysts are structural stability for long term reaction.
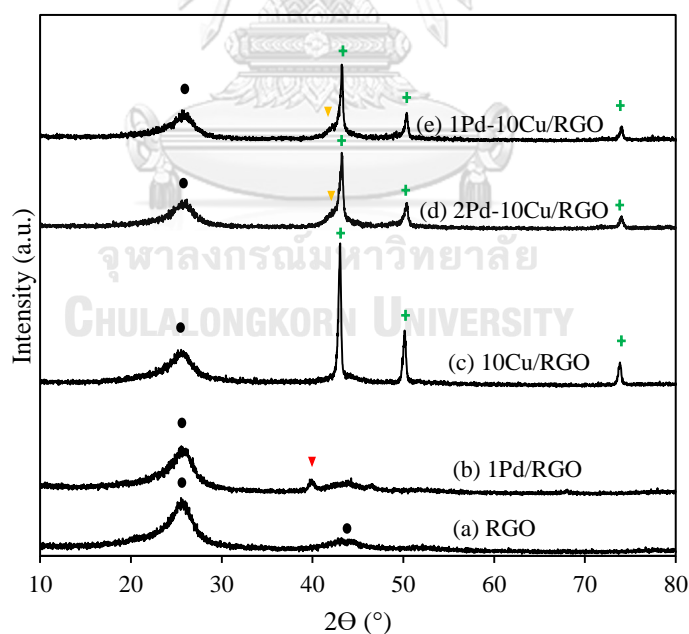
Figure 27 XRD patterns of spent catalysts; (a) RGO, (b) 1Pd/RGO, (c) 10Cu/RGO, (d) 2Pd-10Cu/RGO and (e) 1Pd-10Cu/RGO (symbols assignment: (●) RGO, (▼) Pd^0, (+) Cu^0 and (▼)PdCu$_3$).

Table 6 Crystalline size of the spent catalysts.

Samples	Size of Pd or Cu[a] (nm)	
	Fresh	Spent
RGO	-	-
1Pd/RGO	16	15
10Cu/RGO	29	33
10Cu-1Pd/RGO	19	21
10Cu-2Pd/RGO	23	24

[a]Crystalline size measured from Scherrer equation at (111) plan (Pd; $2\theta= 40.1$, Cu; $2\theta= 43.2$, and Cu+PdCu$_3$; $2\theta= 42.7$-43.2).

4.3.2 X-ray photoelectron spectroscopy (XPS)

In order to analyze the surface electronic state and the component of spent 1Pd-10Cu/RGO catalyst after stability test. The catalyst was further analyzed by XPS. According to the XPS results of fresh monometallic catalysts, the Cu^0 2p$_{3/2}$, Pd^0 3d$_{5/2}$ and Pd^0 3d$_{3/2}$ presented peaks at 932.6 eV, 935.7 eV and 340.8 eV, respectively [85]. For XPS result of spent catalyst, the high resolution XPS spectra of Cu 2p$_{3/2}$ and Pd 3d regions is displayed in Figure 28. In Cu region, the Cu 2p$_{3/2}$ was fitted with two peaks at 932.3 eV and 933.2 eV. Meanwhile, Pd 3d region showed peaks at 335.2 eV and 340.3 eV. These results demonstrated that obtained peaks of spent catalyst (excepted peak of Cu 2p$_{3/2}$ at 933.2 eV) were slightly shifted to lower binding energy as comparison to the peaks of the Cu^0 2p$_{3/2}$, Pd^0 3d$_{5/2}$ and Pd^0 3d$_{3/2}$ of fresh monometallic catalysts, which was probably due to the formation of palladium-copper alloy. Which was agreement with XRD results and other reports [86]. The peak of Cu 2p$_{3/2}$ at 933.2 eV could be attributed to Cu^{2+} [87]. Moreover, a comparison of XPS spectra of fresh and spent 1Pd-10Cu/RGO catalyst in Pd 3d and Cu 2p regions

demonstrated that the oxidation state of copper and palladium was not changed, indicating that the 1Pd-10Cu/RGO catalyst is rather stable for long time reaction
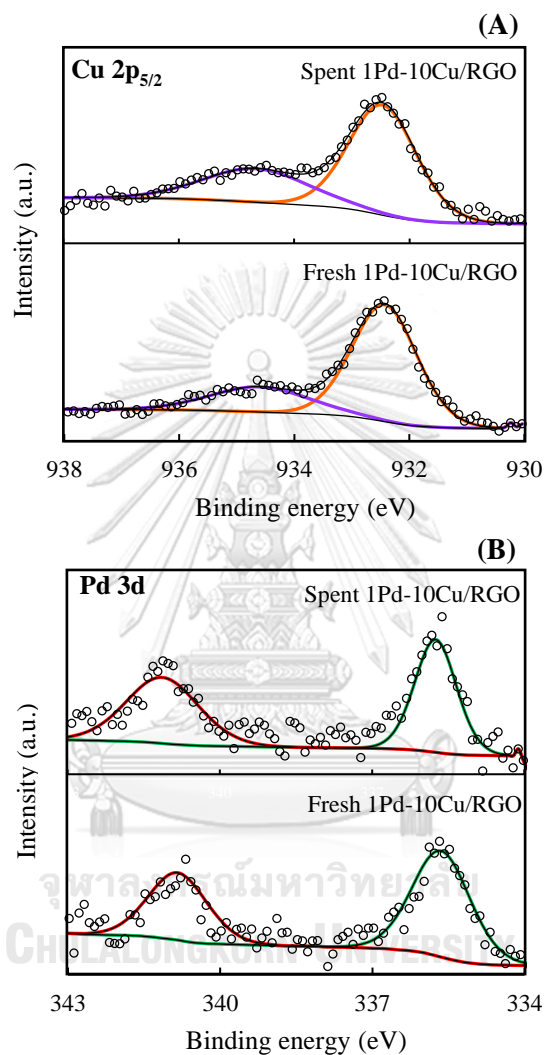
Figure 28 Characterization after stability test of XPS spectra of (A) Cu $2p_{3/2}$ region, and (B) Pd 3d region of the fresh and spent 1Pd-10Cu/RGO catalyst.

4.3.3 Transition electron microscopy (TEM)

TEM micrograph of the spent 1Pd-10Cu/RGO catalyst after stability test is displayed in Figure 29. The palladium-copper alloy was the darker point, while the

RGO support was lighter ones. The catalyst appeared spherical shapes of the alloy clusters decoration on the RGO support. The morphology of spent 1Pd-10Cu/RGO catalyst was maintained after stability tests with no major nanoparticle sintering observed. Moreover, the average cluster size of palladium-copper alloy calculated from TEM micrograph was 19 nm, which was well consistent with the XRD result in Figure 27 and Table 6.
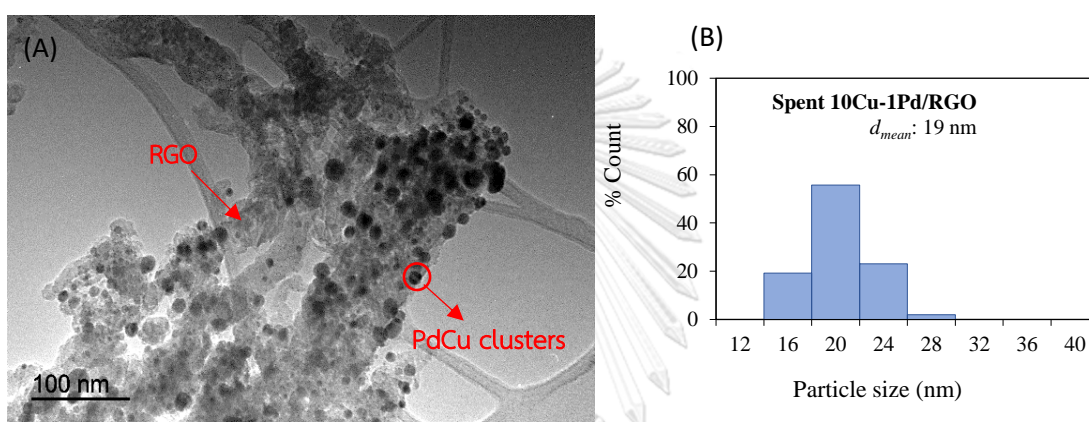
Figure 29 TEM image of (A) spent 1Pd-10Cu/RGO catalysts after stability test with B presents corresponding particle size distribution.

CHAPTER V

CONCLUSION

5.1. Conclusion

The catalytic performance of monometallic (10Cu/RGO and 1Pd/RG) and bimetallic catalysts (1Pd-10Cu/RGO and 2Pd-10Cu/RGO) were studied by using 2-propanol as hydrogen source to achieve a highly efficient catalytic transfer hydrogenation of HMF toward DMF under continuous flow conditions. For monometallic catalysts, 1Pd/RGO catalyst showed low activity (28% HMF conversion) and selectivity to DMF (2.5 % DMF yield) owing to low palladium loading (ca. 1%wt), while 10Cu/RGO catalyst exhibited good activity (60% HMF conversion) and selectivity to DMF (72% DMF selectivity), however; the catalyst presented low catalytic stability due to copper aggregation and copper leaching during the reaction under continuous flow system. XRD results revealed that the cluster size of spent 10Cu/RGO catalysts increased from 29 to 33 nm as compared to fresh catalyst, resulting in low catalytic stability. On the other hand, the bimetallic catalysts exhibited a high HMF conversion and DMF yield (over 85%) as well as good stability as compared to monometallic catalysts. The XRD and XPS results demonstrated the present of palladium-copper alloy, which probably could enhance the catalytic activity and prevent the aggregation of active copper, leading to minimize catalytic deactivation. Moreover, the formation of side products was fully inhibited over bimetallic catalysts. The 1Pd-10Cu/RGO catalyst exhibited a higher activity as compared to 2Pd-10Cu/RGO catalyst due to the smaller crystalline size.

Furthermore, the results found that the HMF conversion and DMF yield increased with temperature increasing, indicating high hydrogenation rate at high temperature (180-200 °C), however; further increases in temperature resulted in over hydrogenolysis leading decreased DMF yield. In addition, the effect of feed flow rate

played an important role in hydrogenation of HMF. The HMF conversion and DMF yield decreased with an increase in flow rate, suggesting that the contact time between reactants and active sites at high flow rate is not sufficient, thus; the thermodynamic equilibrium of the reaction is not completed. Additionally, both HMF conversion and DMF yield also increased upon pressure rising, achieving over 99% of the conversion and DMF yield at 30 bar of pressure. The optimum condition for hydrogenation of HMF toward DMF in continuous flow system over 1Pd-10Cu/RGO catalyst was 180 °C of reaction temperature, 0.2 mL·min^{-1} of flow rate and 15 bar of pressure system.

The optimum system exhibited moderate stability at longer time on stream due to metal leaching (mostly Cu) during the reaction. The alloying of palladium and copper incorporated on reduced graphene oxide support (confirmed with XRD and XPS techniques), was found to have a significant influence in a selective hydrogenation of HMF toward DMF.

5.2 Recommendation

According to the results, it can be seen that the catalytic performance of 1Pd-10Cu/RGO bimetallic catalyst exhibited high activity and selectivity to DMF, however; the main cause of catalyst deactivation under continuous flow system was copper leaching during the reaction, leading moderated stability. Thus, to improve the stability of the catalysts for selective hydrogenation of HMF toward DMF under continuous flow reactor, the addition of basic additive that can increase the interaction between active copper and support, leading to prevent the leaching of active copper during the reaction. The previous studied found that nitrogen doped carbon could enhance the catalytic stability due to strong metal support interaction [31]. Another option to improvement in copper leaching is the developing of catalyst preparation method such as mechanical ball milling, strong electrostatic

adsorption, deposition precipitation methods, which can provide catalyst with strong metal support interaction.

REFERENCES

1. Guillén-Lambea, S.; Rodríguez-Soria, B.; Marín, J. M., Air infiltrations and energy demand for residential low energy buildings in warm climates. *Renewable and Sustainable Energy Reviews* **2019,** *116* (109469), 1-12.

2. Primary energy demand. https://www.naturalgasintel.com, Retrieved November 9, 2019.

3. Tsita, K. G.; Kiartzis, S. J.; Ntavos, N. K.; Pilavachi, P. A., Next generation biofuels derived from thermal and chemical conversion of the Greek transport sector. *Thermal Science and Engineering Progress* **2019.** https://doi.org/10.1016/j.tsep. 2019.100387.

4. CO_2: Earth's thermostat is set higher. https://1wow.org/blog/co2-earth-thermo-statset-higher, Retrieved November 9, 2019.

5. Tanzer, S. E.; Posada, J.; Geraedts, S.; Ramírez, A., Lignocellulosic marine biofuel: Technoeconomic and environmental assessment for production in Brazil and Sweden. *Journal of Cleaner Production* **2019,** *239* (117845), 1-15.

6. Kesharwani, R.; Sun, Z.; Dagli, C.; Xiong, H., Moving second generation biofuel manufacturing forward: Investigating economic viability and environmental sustainability considering two strategies for supply chain restructuring. *Applied Energy* **2019,** *242,* 1467-1496.

7. Biofuel and bioenergy. http://refuelingthefuture.yolasite.com/biofuels-and-bio-energy.php, Retrieved November 9, 2019.

8. Hu, L.; Lin, L.; Wu, Z.; Zhou, S.; Liu, S., Recent advances in catalytic transformation of biomass-derived 5-hydroxymethylfurfural into the innovative fuels and chemicals. *Renewable and Sustainable Energy Reviews* **2017,** *74,* 230-257.

9. Wang, X.; Liang, X.; Li, J.; Li, Q., Catalytic hydrogenolysis of biomass-derived 5-hydroxymethylfurfural to biofuel 2, 5-dimethylfuran. *Applied Catalysis A: General*

2019, *576,* 85-95.

10. Wang, H.; Zhu, C.; Li, D.; Liu, Q.; Tan, J.; Wang, C.; Cai, C.; Ma, L., Recent advances in catalytic conversion of biomass to 5-hydroxymethylfurfural and 2,5-dimethylfuran. *Renewable and Sustainable Energy Reviews* **2019,** *103,* 227-247.

11. Xu, H.; Wang, C., A Comprehensive review of 2,5-dimethylfuran as a biofuel candidate. In *Biofuels from Lignocellulosic Biomass,* **2016,** 105-129.

12. Tang, X.; Wei, J.; Ding, N.; Sun, Y.; Zeng, X.; Hu, L.; Liu, S.; Lei, T.; Lin, L., Chemoselective hydrogenation of biomass derived 5-hydroxymethylfurfural to diols: Key intermediates for sustainable chemicals, materials and fuels. *Renewable and Sustainable Energy Reviews* **2017,** *77,* 287-296.

13. Chen, B.; Li, F.; Huang, Z.; Yuan, G., Carbon-coated Cu-Co bimetallic nanoparticles as selective and recyclable catalysts for production of biofuel 2,5-dimethylfuran. *Applied Catalysis B: Environmental* **2017,** *200,* 192-199.

14. Luo, J.; Arroyo-Ramírez, L.; Wei, J.; Yun, H.; Murray, C. B.; Gorte, R. J., Comparison of HMF hydrodeoxygenation over different metal catalysts in a continuous flow reactor. *Applied Catalysis A: General* **2015,** *508,* 86-93.

15. Nakagawa, Y.; Tamura, M.; Tomishige, K., Supported Metal Catalysts for Total Hydrogenation of Furfural and 5-Hydroxymethylfurfural. *Journal of the Japan Petroleum Institute* **2017,** *60* (1), 1-9.

16. Gilkey, M. J.; Xu, B., Heterogeneous catalytic transfer hydrogenation as an effective pathway in biomass upgrading. *ACS Catalysis* **2016,** *6* (3), 1420-1436.

17. Zhang, J.; Dong, K.; Luo, W., PdCl$_2$-catalyzed hydrodeoxygenation of 5-hydroxymethylfurfural into 2,5-dimethylfuran at room-temperature using poly-methylhydrosiloxane as the hydrogen donor. *Chemical Engineering Science* **2019,** *201,* 467-474.

18. Gupta, K.; Rai, R. K.; Singh, S. K., Metal catalysts for the efficient transformation of

biomass-derived HMF and furfural to value added chemicals. *ChemCatChem* **2018,** *10* (11), 2326-2349.

19. Chen, N.; Zhu, Z.; Su, T.; Liao, W.; Deng, C.; Ren, W.; Zhao, Y.; Lü, H., Catalytic hydrogenolysis of hydroxymethylfurfural to highly selective 2,5-dimethylfuran over FeCoNi/h-BN catalyst. *Chemical Engineering Journal* **2020,** *381* (122755), 1-7.

20. Chatterjee, M.; Ishizaka, T.; Kawanami, H., Hydrogenation of 5-hydroxymethy-lfurfural in supercritical carbon dioxide-water: A tunable approach to dimethylfuran selectivity. *Green Chemistry* **2014,** *16* (3), 1543-15551.

21. Mitra, J.; Zhou, X.; Rauchfuss, T., Pd/C-catalyzed reactions of HMF: Decarbo-nylation, hydrogenation, and hydrogenolysis. *Green Chemistry* **2015,** *17* (11), 307-313.

22. Gawade, A. B.; Tiwari, M. S.; Yadav, G. D., Biobased green process: selective hydrogenation of 5-hydroxymethylfurfural to 2,5-dimethyl furan under mild conditions using Pd-Cs$_{2.5}$H$_{0.5}$PW$_{12}$O$_{40}$/K-10 clay. *ACS Sustainable Chemistry and Engineering* **2016,** *4* (8), 4113-4123.

23. Jae, J.; Zheng, W.; Lobo, R. F.; Vlachos, D. G., Production of dimethylfuran from hydroxymethylfurfural through catalytic transfer hydrogenation with ruthenium supported on carbon. **2013,** *6* (7), 1158-1162.

24. Priecel, P.; Endot, N. A.; Carà, P. D.; Lopez-Sanchez, J. A., Fast Catalytic hydrogenation of 2,5-hydroxymethylfurfural to 2,5-dimethylfuran with ruthenium on carbon nanotubes. *Industrial and Engineering Chemistry Research* **2018,** *57* (6), 1991-2002.

25. Nagpure, A. S.; Venugopal, A. K.; Lucas, N.; Manikandan, M.; Thirumalaiswamy, R.; Chilukuri, S., Renewable fuels from biomass-derived compounds: Ru-containing hydrotalcites as catalysts for conversion of HMF to 2,5-dimethylfuran. *Catalysis Science and Technology* **2015,** *5* (3), 1463-1472.

26. Zu, Y.; Yang, P.; Wang, J.; Liu, X.; Ren, J.; Lu, G.; Wang, Y., Efficient production of the liquid fuel 2,5-dimethylfuran from 5-hydroxymethylfurfural over Ru/Co$_3$O$_4$ catalyst. *Applied Catalysis B: Environmental* **2014,** *146,* 244-248.

27. Yang, Y.; Liu, Q.; Li, D.; Tan, J.; Zhang, Q.; Wang, C.; Ma, L., Selective hydrodeoxygenation of 5-hydroxymethylfurfural to 2,5-dimethylfuran on Ru-MoO$_x$/C catalysts. *RSC Advances* **2017,** *7* (27), 16311-16318.

28. Yang, P.; Xia, Q.; Liu, X.; Wang, Y., Catalytic transfer hydrogenation/ hydroge-nolysis of 5-hydroxymethylfurfural to 2,5-dimethylfuran over Ni-Co/C catalyst. *Fuel* **2017,** *187,* 159-166.

29. Román-Leshkov, Y.; Barrett, C. J.; Liu, Z. Y.; Dumesic, J. A., Production of di-methylfuran for liquid fuels from biomass-derived carbohydrates. *Nature* **2007,** *447* (7147), 982-985.

30. Iriondo, A.; Mendiguren, A.; Güemez, M. B.; Requies, J.; Cambra, J. F., 2,5-DMF production through hydrogenation of real and synthetic 5-HMF over transition metal catalysts supported on carriers with different nature. *Catalysis Today* **2017,** *279,* 286-295.

31. Gao, Z.; Li, C.; Fan, G.; Yang, L.; Li, F., Nitrogen-doped carbon-decorated copper catalyst for highly efficient transfer hydrogenolysis of 5-hydroxymethylfurfural to convertibly produce 2,5-dimethylfuran or 2,5-dimethyltetrahydrofuran. *Applied Catalysis B: Environmental* **2018,** *226,* 523-533.

32. Kong, X.; Zhu, Y.; Zheng, H.; Li, X.; Zhu, Y.; Li, Y. W., Ni Nanoparticles inlaid nickel phyllosilicate as a metal-acid bifunctional catalyst for low-temperature hydrogenolysis reactions. *ACS Catalysis* **2015,** *5* (10), 5914-5920.

33. Gyngazova, M. S.; Negahdar, L.; Blumenthal, L. C.; Palkovits, R., Experimental and kinetic analysis of the liquid phase hydrodeoxygenation of 5-hydroxymethyl-furfural to 2,5-dimethylfuran over carbon-supported nickel catalysts. *Chemical Engineering*

Science **2017,** *173*, 455-464.

34. Huang, Y.-B.; Chen, M. Y.; Yan, L.; Guo, Q. X.; Fu, Y., Nickel-tungsten carbide catalysts for the production of 2,5-dimethylfuran from biomass-derived molecules. *ChemSusChem* **2014,** *7* (4), 1068-1072.

35. Qian, J.; Hou, X.; Qin, Z.; Li, B.; Tong, Z.; Dong, L.; Dong, L., Enhanced catalytic properties of Cu-based composites for NO_x reduction with coexistence and intergrowth effect. *Fuel* **2018,** *234*, 296-304.

36. Kumalaputri, A. J.; Bottari, G.; Erne, M. P.; Heeres, J. H.; Barta, K., Tunable and selective conversion of 5-HMF to 2,5-furandimethanol and 2,5-dimethylfuran over copper-doped porous metal oxides. *ChemSusChem* **2014,** *7* (8). 1201-1222.

37. Román-Leshkov, Y.; Barrett, C. J.; Liu, Z. Y.; Dumesic, J. A., Production of dimethylfuran for liquid fuels from biomass-derived carbohydrates. *Nature* **2007,** *447* (7147), 982-985.

38. Chen, J.; Ge, Y.; Guo, Y.; Chen, J., Selective hydrogenation of biomass-derived 5-hydroxymethylfurfural using palladium catalyst supported on mesoporous graphitic carbon nitride. *Journal of Energy Chemistry* **2018,** *27* (1), 283-289.

39. Hronec, M.; Fulajtárová, K.; Vávra, I.; Soták, T.; Dobročka, E.; Mičušík, M., Carbon supported Pd-Cu catalysts for highly selective rearrangement of furfural to cyclopentanone. *Applied Catalysis B: Environmental* **2016,** *181*, 210-219.

40. Srivastava, S.; Jadeja, G. C.; Parikh, J., Synergism studies on alumina-supported copper-nickel catalysts towards furfural and 5-hydroxymethylfurfural hydro-genation. *Journal of Molecular Catalysis A: Chemical* **2017,** *426*, 244-256.

41. Fulajtárova, K.; Soták, T.; Hronec, M.; Vávra, I.; Dobročka, E.; Omastová, M., Aqueous phase hydrogenation of furfural to furfuryl alcohol over Pd-Cu catalysts. *Applied Catalysis A: General* **2015,** *502*, 78-85.

42. Fu, Z.; Wang, Z.; Lin, W.; Song, W.; Li, S., High efficient conversion of furfural to 2-

methylfuran over Ni-Cu/Al$_2$O$_3$ catalyst with formic acid as a hydrogen donor. *Applied Catalysis A: General* **2017,** *547*, 248-255.

43. Ye, B.; Lee, M.; Jeong, B.; Kim, J.; Lee, D. H.; Baik, J. M.; Kim, H.-D., Partially reduced graphene oxide as a support of Mn-Ce/TiO$_2$ catalyst for selective catalytic reduction of NO$_x$ with NH$_3$. *Catalysis Today* **2019,** *328*, 300-306.

44. Zheng, X.; Zhao, J.; Xu, M.; Zeng, M., Preparation of porous chitosan/reduced graphene oxide microspheres supported Pd nanoparticles catalysts for Heck coupling reactions. *Carbohydrate Polymers* **2019**. https://doi.org/10.1016/j.carb-pol.2019.115583.

45. Hu, F.; Tong, S.; Lu, K.; Chen, C.-M.; Su, F.-Y.; Zhou, J.; Lu, Z.-H.; Wang, X.; Feng, G.; Zhang, R., Reduced graphene oxide supported Ni-Ce catalysts for CO$_2$ methanation: The support and ceria promotion effects. *Journal of CO$_2$ Utilization* **2019,** *34*, 676-687.

46. Rowley-Neale, S. J.; Randviir, E. P.; Abo Dena, A. S.; Banks, C. E., An overview of recent applications of reduced graphene oxide as a basis of electroanalytical sensing platforms. *Applied Materials Today* **2018,** *10*, 218-226.

47. Ismail, Z., Green reduction of graphene oxide by plant extracts: A short review. *Ceramics International* **2019,** *45* (18), 23857-23868.

48. Li, B.; Yan, Q.; Song, C.; Yan, P.; Ye, K.; Cheng, K.; Zhu, K.; Yan, J.; Cao, D.; Wang, G., Reduced graphene oxide foam supported CoNi nanosheets as an efficient anode catalyst for direct borohydride hydrogen peroxide fuel cell. *Applied Surface Science* **2019,** *491*, 659-669.

49. Navalon, S.; Dhakshinamoorthy, A.; Alvaro, M.; Garcia, H., Metal nanoparticles supported on two-dimensional graphenes as heterogeneous catalysts. *Coordination Chemistry Reviews* **2016,** *312*, 99-148.

50. Wang, Y.; Prinsen, P.; Triantafyllidis, K. S.; Karakoulia, S. A.; Yepez, A.; Len, C.;

Luque, R., Batch versus continuous flow performance of supported mono- and bimetallic nickel catalysts for catalytic transfer hydrogenation of furfural in isopropanol. *ChemCatChem* **2018,** *10* (16), 3459-3468.

51. Lázaro, N.; Franco, A.; Ouyang, W.; Balu, A.; Romero, A.; Luque, R.; Pineda, A., Continuous-flow hydrogenation of methyl levulinate promoted by Zr-based mesoporous materials. *Catalysts* **2019,** *9* (2), 1201-1221.

52. Garcia-Olmo, A. J.; Yepez, A.; Balu, A. M.; Prinsen, P.; Garcia, A.; Maziere, A.; Len, C.; Luque, R., Activity of continuous flow synthesized Pd-based nanocatalysts in the flow hydroconversion of furfural. *Tetrahedron* **2017,** *73* (38), 5599-5604.

53. Wang, Y.; Prinsen, P.; Triantafyllidis, K. S.; Karakoulia, S. A.; Trikalitis, P. N.; Yepez, A.; Len, C.; Luque, R., Comparative study of supported monometallic catalysts in the liquid-phase hydrogenation of furfural: batch versus continuous flow. *ACS Sustainable Chemistry & Engineering* **2018,** *6* (8), 9831-9844.

54. Zhang, Z.; Wang, C.; Gou, X.; Chen, H.; Chen, K.; Lu, X.; Ouyang, P.; Fu, J., Catalytic in-situ hydrogenation of 5-hydroxymethylfurfural to 2,5-dimethylfuran over Cu-based catalysts with methanol as a hydrogen donor. *Applied Catalysis A: General* **2019,** *570*, 245-250.

55. Du, J.; Zhang, J.; Sun, Y.; Jia, W.; Si, Z.; Gao, H.; Tang, X.; Zeng, X.; Lei, T.; Liu, S.; Lin, L., Catalytic transfer hydrogenation of biomass-derived furfural to furfuryl alcohol over in-situ prepared nano Cu-Pd/C catalyst using formic acid as hydrogen source. *Journal of Catalysis* **2018,** *368*, 69-78.

56. Nishimura, S.; Ikeda, N.; Ebitani, K., Selective hydrogenation of biomass-derived 5-hydroxymethylfurfural (HMF) to 2,5-dimethylfuran (DMF) under atmospheric hydrogen pressure over carbon supported PdAu bimetallic catalyst. *Catalysis Today* **2014,** *232*, 89-98.

57. Fulignati, S.; Antonetti, C.; Licursi, D.; Pieraccioni, M.; Wilbers, E.; Heeres, H. J.;

Raspolli Galletti, A. M., Insight into the hydrogenation of pure and crude HMF to furan diols using Ru/C as catalyst. *Applied Catalysis A: General* **2019,** *578*, 122-133.

58. Ouyang, W.; Yepez, A.; Romero, A. A.; Luque, R., Towards industrial furfural conversion: Selectivity and stability of palladium and platinum catalysts under continuous flow regime. *Catalysis Today* **2018,** *308*, 32-37.

59. Lowell S., S. E. J., Thomas A.M., Thomas M., Characterization f porous solids and powders: surfce area, pore size and density. Kluwer Academic: Natherlands, **2004,** 2-80.

60. ASAP 2020 accelerated surface area and porosimetry system. https://www.micro-meritics.com/Repository/Files/ASAP_2020., Retrieved November 9, 2019.

61. Instrumentation and methods. Luyberg, M., Tillmann, K., Weirich T., Ed. Springer: Germany, **2008**, 93-121.

62. JSM-7800F schottky field emission scanning electron microscope. https://www. jeol.co.jp/en/products/detail/JSM-7800F.html., Retrieved November 9, 2019.

63. X-ray diffraction imaging: technology and applications. Iniewaki, K., Ed. Taylor and Francies Group CRC Press: 2018.

64. Technology of materials. http://www.xraydiffrac.com/xraydiff.html., Retrieved November 9, 2019.

65. D8 ADVANCE X-ray diffractometer from Bruker. https://www.americanpharmaceu-ticalreview.com, Retrieved November 9, 2019.

66. Douglas A. Skoog, F. J. H., Stanley R. Crouch, Principles of instrumental analysis. USA, **2016**, 541-560.

67. Electronic properties of materials. https://epm.univie.ac.at/research/low-dimen-sional-quantum-solids/methods., Retrieved November 9, 2019.

68. Photoelectron spectroscopy system. http://www specs-group. com/ nc/ specs/ products/detail/photoelectron-spectroscopy, Retrieved November 9, 2019.

69. Savile Bradbury, D. C. J., Brian J. Ford Transmission electron microscope instrument. https://www.britannica.com/technology/transmission-electronmicro-scope., Retrieved November 9, 2019.

70. FEI Tecnai G^2 Spirit Twin TEM. https://asrc.gc.cuny.edu/nanoscience/facilities/ imaging-facility/instrument, Retrieved November 9, 2019.

71. Automated catalyst characterization system -AutoChem II 2920. https://www. micromeritics.com/Product-Showcase/AutoChem-II-2920., Retrieved November 9, 2019.

72. Phoenix Flow Reactor. https://thalesnanocomproducts-and-servicesphoenix-flow-reactor, Retrieved November 9, 2019.

73. Deng, F.; Pei, X.; Luo, Y.; Luo, X.; Dionysiou, D.; Wu, S.; Luo, S., Fabrication of hierarchically porous reduced graphene oxide/$SnIn_4S_8$ composites by a low-temperature co-precipitation strategy and their excellent visible-light photo-catalytic mineralization performance. *Catalysts* **2016,** *6* (8), 201-208.

74. Díez-Ramírez, J.; Díaz, J. A.; Sánchez, P.; Dorado, F., Optimization of the Pd/Cu ratio in Pd-Cu-Zn/SiC catalysts for the CO_2 hydrogenation to methanol at atmospheric pressure. *Journal of CO_2 Utilization* **2017,** *22*, 71-80.

75. Jiang, X.; Koizumi, N.; Guo, X.; Song, C., Bimetallic Pd–Cu catalysts for selective CO_2 hydrogenation to methanol. *Applied Catalysis B: Environmental* **2015,** *170-171*, 173-185.

76. Jiang, X.; Nie, X.; Wang, X.; Wang, H.; Koizumi, N.; Chen, Y.; Guo, X.; Song, C., Origin of Pd-Cu bimetallic effect for synergetic promotion of methanol formation from CO_2 hydrogenation. *Journal of Catalysis* **2019,** *369*, 21-32.

77. Gholinejad, M.; Bahrami, M.; Nájera, C.; Pullithadathil, B., Magnesium oxide supported bimetallic Pd/Cu nanoparticles as an efficient catalyst for Sonogashira reaction. *Journal of Catalysis* **2018,** *363*, 81-91.

78. Shi, R.; Ren, M.; Li, H.; Zhao, J.; Liu, S.; Li, Z.; Ren, J., Graphene supported Cu nanoparticles as catalysts for the synthesis of dimethyl carbonate: Effect of carbon black intercalation. *Molecular Catalysis* **2018,** *445*, 257-268.

79. Fox, E. B.; Velu, S.; Engelhard, M. H.; Chin, Y.-H.; Miller, J. T.; Kropf, J.; Song, C., Characterization of CeO_2-supported Cu-Pd bimetallic catalyst for the oxygen-assisted water-gas shift reaction. *Journal of Catalysis* **2008,** *260* (2), 358-370.

80. Yoshida, K.; Gonzalez-Arellano, C.; Luque, R.; Gai, P. L., Efficient hydrogenation of carbonyl compounds using low-loaded supported copper nanoparticles under microwave irradiation. *Applied Catalysis A: General* **2010,** *379* (1-2), 38-44.

81. Sitthisa, S.; Pham, T.; Prasomsri, T.; Sooknoi, T.; Mallinson, R. G.; Resasco, D. E., Conversion of furfural and 2-methylpentanal on Pd/SiO_2 and $Pd–Cu/SiO_2$ catalysts. *Journal of Catalysis* **2011,** *280* (1), 17-27.

82. Lesiak, M.; Binczarski, M.; Karski, S.; Maniukiewicz, W.; Rogowski, J.; Szubiakiewicz, E.; Berlowska, J.; Dziugan, P.; Witońska, I., Hydrogenation of furfural over Pd–Cu/Al_2O_3 catalysts. The role of interaction between palladium and copper on determining catalytic properties. *Journal of Molecular Catalysis A: Chemical* **2014,** *395*, 337-348.

83. Zhou, F.; Du, X.; Yu, J.; Mao, D.; Lu, G., Highly water-resistant carbon nanotube supported $PdCl_2$–$CuCl_2$ catalysts for low temperature CO oxidation. *RSC Advances* **2016,** *6* (71), 66553-66563.

84. Srivastava, S.; Jadeja, G. C.; Parikh, J., Influence of supports for selective production of 2,5-dimethylfuran *via* bimetallic copper-cobalt catalyzed 5-hydroxymethylfurfural hydrogenolysis. *Chinese Journal of Catalysis* **2017,** *38* (4), 699-709.

85. Yang, F.; Zhang, B.; Dong, S.; Wang, C.; Feng, A.; Fan, X.; Li, Y., Reduced graphene oxide supported Pd-Cu-Co trimetallic catalyst: synthesis, charac-terization and

methanol electrooxidation properties. *Journal of Energy Chemistry* **2019,** *29*, 72-78.

86. Cheah, K. W.; Taylor, M. J.; Osatiashtiani, A.; Beaumont, S. K.; Nowakowski, D. J.; Yusup, S.; Bridgwater, A. V.; Kyriakou, G., Monometallic and bimetallic catalysts based on Pd, Cu and Ni for hydrogen transfer deoxygenation of a prototypical fatty acid to diesel range hydrocarbons. *Catalysis Today* **2019**.

87. Zhang, Z.; Yao, S.; Wang, C.; Liu, M.; Zhang, F.; Hu, X.; Chen, H.; Gou, X.; Chen, K.; Zhu, Y.; Lu, X.; Ouyang, P.; Fu, J., CuZnCoO$_x$ multifunctional catalyst for in situ hydrogenation of 5-hydroxymethylfurfural with ethanol as hydrogen carrier. *Journal of Catalysis* **2019,** *373*, 314-321.
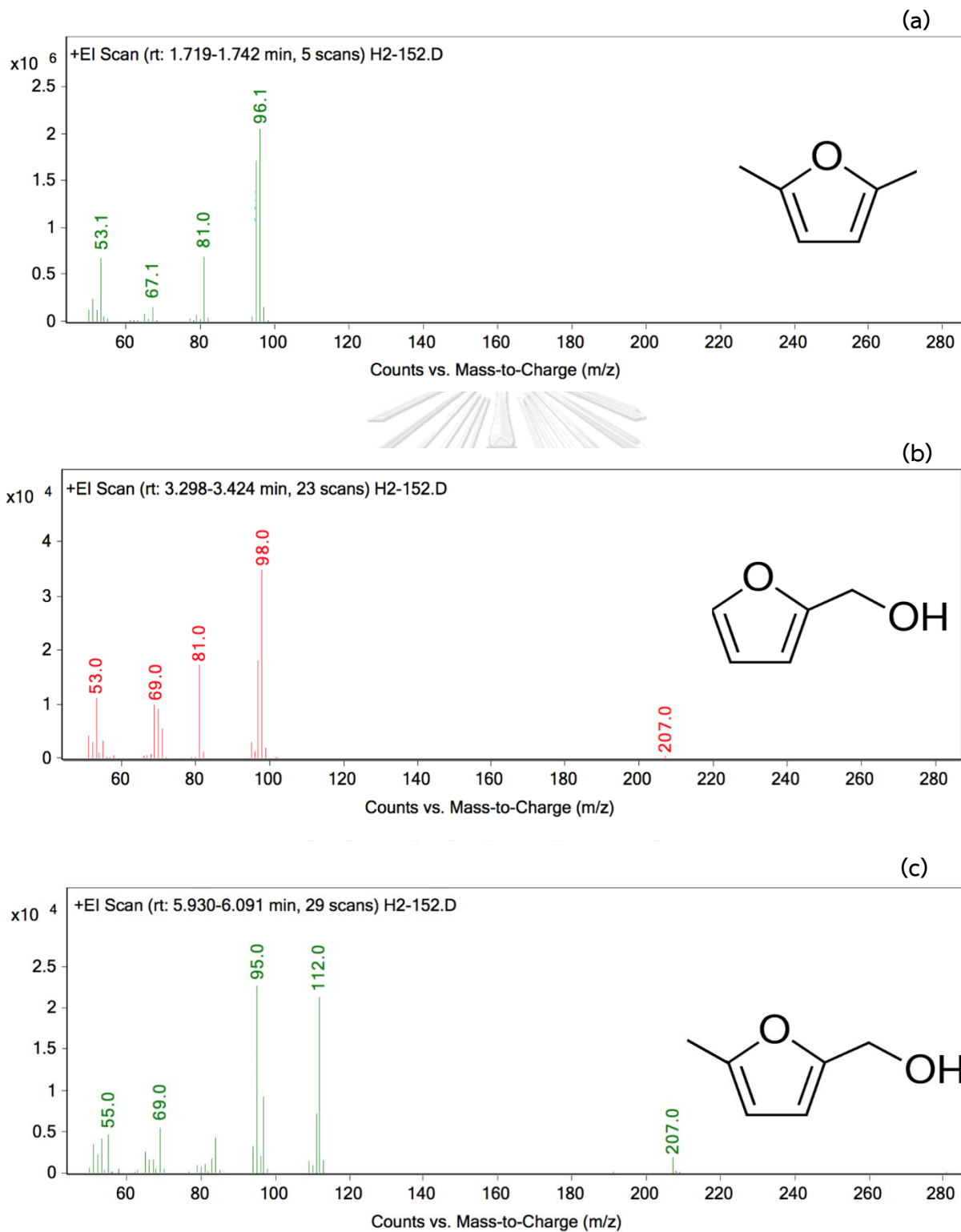
APPENDIX

Appendix A

Figure-A1 MS spectra of hydrogenated products: (a) DMF, (b) FA and (c) MFA.
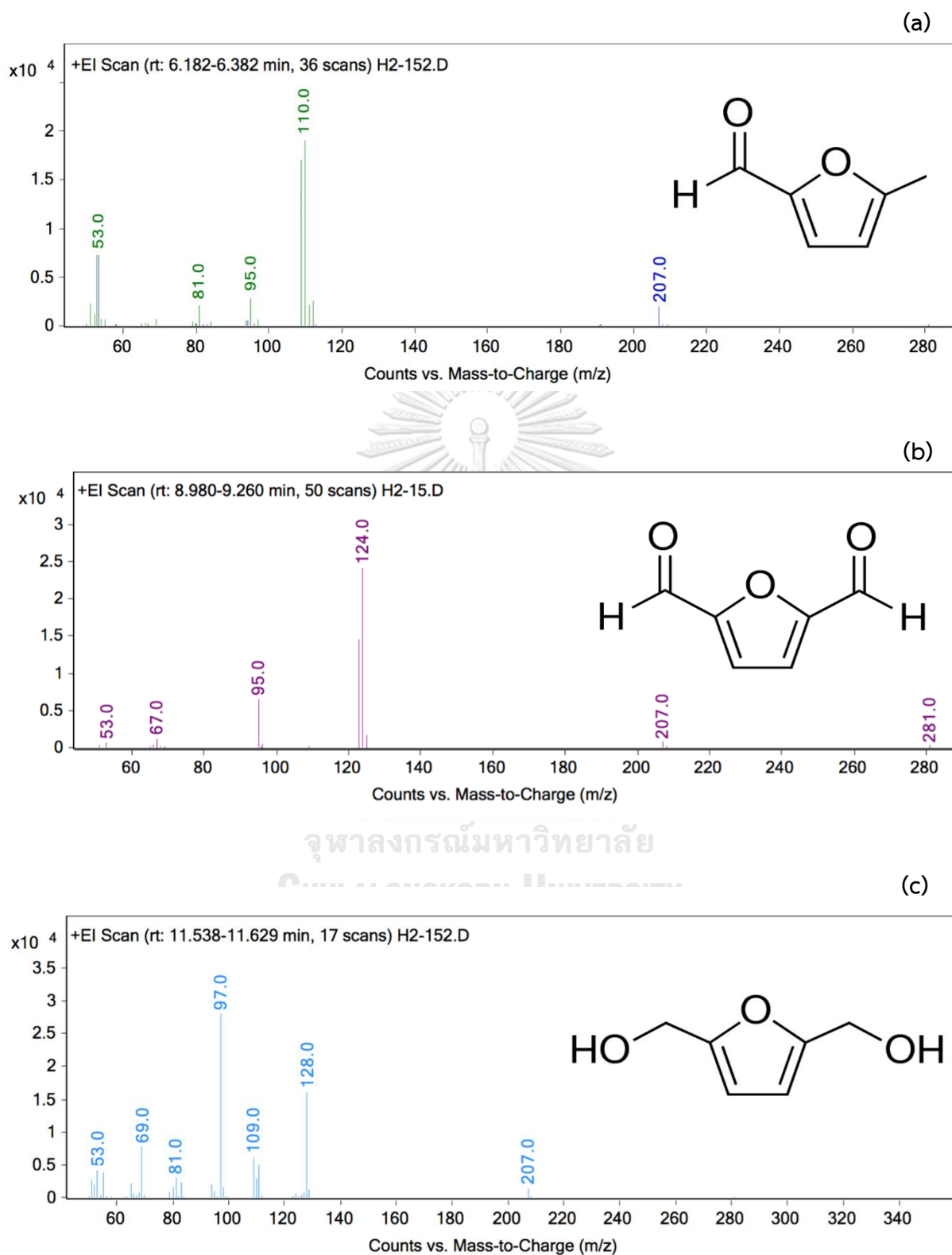
Figure-A2 MS spectra of hydrogenated products: (a) MF, (b) MFF and (c) DHMF.

Appendix B

Calculation

1. Calculation for metal loading

   1.1 10 %wt Cu loading (10Cu/RGO catalyst)

   Cu precursor; $(CH_3COO)_2Cu \cdot H_2O$

   Cu (MW = 63.5 g/mol)

   $(CH_3COO)_2Cu \cdot H_2O$ (MW = 199.65 g/mol)

   Basis 0.9 g of RGO

       Cu = (10x0.9)/90 = 0.1 g

       Weight of $(CH_3COO)_2Cu \cdot H_2O$ = (0.1x199.65)/63.5 = 0.3144 g

   1.2 1 %wt Pd loading (1Pd/RGO catalyst)

   Pd precursor; $Pd(CH_3COO)_2$

   Pd (MW = 106.4 g/mol)

   $Pd(CH_3COO)_2$ (MW = 224.51 g/mol)

   Basis 0.99 g of RGO

       Pd = (1x0.99)/99 = 0.01 g

       Weight of $Pd(CH_3COO)_2$= (0.01x224.51)/106.4 = 0.0211 g

   1.3 1 %wt Pd and 10 %wt Cu loading (1Pd-10Cu/RGO catalyst)

   Basis 0.89 g of RGO

   Pd = 0.01 g

   Cu = 0.10 g

       Weight of $Pd(CH_3COO)_2$= (0.01x224.51)/106.4 = 0.0211 g

       Weight of $(CH_3COO)_2Cu \cdot H_2O$ = (0.1x199.65)/63.5 = 0.3144 g

   1.3 2 %wt Pd and 10 %wt Cu loading (2Pd-10Cu/RGO catalyst)

   Basis 0.88 g of RGO

   Pd = 0.02 g

   Cu = 0.10 g

Weight of Pd(CH₃COO)₂= (0.02x224.51)/106.4 = 0.0422 g

Weight of (CH₃COO)₂Cu·H₂O = (0.1x199.65)/63.5 = 0.3144 g

2. Hydrogenation reaction

$$X_{(HMF)} = \frac{c_{in} - c_{out}}{c_{in}} \times 100 \qquad (1)$$

When c_{in} = Molar flow rate of 5-hydroxymethylfurfural inlet (μmol·mL⁻¹)

c_{out} = Molar flow rate of 5-hydroxymethylfurfural outlet (μmol·mL¹)

$X_{(HMF)}$ = conversion of 5-hydroxymethylfurfural (%)

$$S_{(i)} = \frac{c_i}{c_{in} - c_{out}} \times 100 \qquad (2)$$

Where c_i = Molar flow rate of the products, including DFF, DHMF, MF,

MFA, FA and DMF (μmol·mL⁻¹)

$S_{(i)}$ = Selectivity of products (%)

$$Y_{(i)} = \frac{X_{(HMF)} \times S_{(i)}}{100} \qquad (3)$$

When $Y_{(i)}$ = Yield of products (%)

For example,

Reaction condition: 0.05 M HMF in 2- propanol, 160 °C, 0.2 mL·min⁻¹ and 30 bar
at 2h. Catalyst = 0.110 g, 0.0075 mmol·mL⁻¹ of n-octane in sample outlet

	Area Sample	Response factor
DMF	3980441.10	0.71
FA	807119.67	0.85
MFA	728454.63	1.10
MF	608732.75	0.92
HMF	11017906.91	1.21
IS	2547812.01	

Therefore

C_{DMF} = (0.0075 mmol·mL^{-1} x 3980441.10 x 0.2 mL·min^{-1})/(0.71 x 2547812.01)

       = 3.301 µmol·min^{-1}

C_{FA} = (0.0075 mmol·mL^{-1} x 807119.67x 0.2 mL·min^{-1})/(0.85 x 2547812.01)

       = 0.559 µmol·min^{-1}

C_{MFA} = (0.0075 mmol·mL^{-1} x 728454.63 x 0.2 mL·min^{-1})/(1.10 x 2547812.01)

       = 0.389 µmol·min^{-1}

C_{MF} = (0.0075 mmol·mL^{-1} x 608732.75 x 0.2 mL·min^{-1})/(0.92 x 2547812.01)

       = 0.389 µmol·min^{-1}

C_{out} = (0.075 mmol·mL^{-1} x 11017906.91 x 0.2 mL·min^{-1})/(1.21 x 2547812.01)

       = 5.361 µmol·min^{-1}

C_{in} = (0.05 mol·L^{-1} x 24.3 mL)/120 min = 10.125 µmol·min^{-1}

Therefore

$X_{(HMF)}$ = ((10.125 − 5.361)/10.125) x 100 = 47.05 %

S_{DMF} = (3.301/(10.125 − 5.361)) x 100 = 71.15 %

S_{FA} = (0.559/(10.125 − 5.361)) x 100 = 12.05 %

S_{MFA} = (0.3989/(10.125 − 5.361)) x 100 = 8.40 %

S_{MF} = (0.389/(10.125 − 5.361)) x 100 = 8.40 %

Y_{DMF} = (47.05 x 71.15)/100 = 33.48 %

Y_{FA} = (47.05 x 12.05)/100 = 5.67 %

Y_{MMF} = (47.05 x 8.40)/100 = 3.95 %

Y_{MF} = (47.05 x 8.40)/100 = 3.95 %

VITA

NAME	Sareena Mhadmhan
DATE OF BIRTH	01 Feb 1991
PLACE OF BIRTH	Phatthalung Thailand
INSTITUTIONS ATTENDED	Chulalongkorn university
HOME ADDRESS	382/2 Nongthong, Pa Bon, Phatthalung 93170
PUBLICATION	Mhadmhan, S.; Franco, A.; Pineda, A.; Reubroycharoen, P.; Luque, R., Continuous Flow Selective Hydrogenation of 5-Hydroxymethylfurfural to 2,5-Dimethylfuran Using Highly Active and Stable Cu–Pd/Reduced Graphene Oxide. ACS Sustainable Chemistry & Engineering 2019, 7 (16), 14210-14216.

จุฬาลงกรณ์มหาวิทยาลัย
CHULALONGKORN UNIVERSITY